Ecdysone regulates the *Drosophila* imaginal disc epithelial barrier, determining the duration of regeneration checkpoint delay

Danielle DaCrema, Rajan Bhandari, Faith Karanja, Ryunosuke Yano, Adrian Halme*

Key words: Epithelial Barrier, Septate Junction, Regeneration, Dilp8, Ecdysone, Coracle

Department of Cell Biology
University of Virginia School of Medicine
Charlottesville, VA 22902

*Corresponding Author: ajh6a@virginia.edu

Summary Statement

Ecdysone signaling directs the *Drosophila* third instar imaginal disc epithelial barrier to mature, becoming more restrictive. This mature barrier limits Dilp8 signaling and determines the duration of the regeneration checkpoint.

Abstract

Regeneration of *Drosophila* imaginal discs, larval precursors to adult tissues, produces a systemic response, a regeneration checkpoint that coordinates regenerative growth with developmental progression. This regeneration checkpoint is coordinated by the release of the relaxin-family peptide Dilp8 from regenerating tissues. Secreted Dilp8 protein can be detected within the imaginal disc lumen. The disc epithelium separates from the lumen from the larval hemolymph and the targets for Dilp8 activity in the brain and prothoracic gland. Here we demonstrate that the imaginal disc epithelial barrier limits Dilp8 signaling and checkpoint delay. We also observe that the wing imaginal disc barrier becomes more restrictive during development, becoming impermeable only at end of the final larval instar. This change in barrier permeability is driven by the steroid hormone ecdysone and correlates with changes in localization of Coracle, a component of the septate junctions that is required for the late, impermeable epithelial barrier. Based on these observations, we propose that the imaginal disc epithelial barrier regulates the duration of the regenerative checkpoint, providing a mechanism by which tissue function can signal the completion of regeneration.

Introduction

Drosophila melanogaster imaginal discs, larval precursors to adult organs, can regenerate after damage early in development, but lose this regenerative ability to prior to pupariation (Halme et al., 2010). Following damage, regenerating imaginal discs activate a regeneration checkpoint through release of the relaxin peptide *Drosophila* insulin-like peptide 8 (Dilp8) (Colombani et al., 2012; Garelli et al., 2012). Dilp8 functions in the brain and the prothoracic gland (PG) by binding to the relaxin receptor (Lgr3), which inhibits the synthesis of the steroid hormone ecdysone (Colombani et al., 2015; Garelli et al., 2015; Jaszczak et al., 2016; Vallejo et al., 2015). Ecdysone triggers many of the developmental events that characterize the end of larval development and pupariation, including regeneration restriction (Hackney and Cherbas, 2014; Halme et al., 2010). Therefore, the inhibition of ecdysone synthesis during the regeneration checkpoint extends the larval phase, coordinating regeneration with developmental progression (Halme et al., 2010; Jaszczak et al., 2016). However, it is unclear what events determine the duration of the regenerative checkpoint and signal the completion of regeneration, allowing the larvae to enter pupation and progress through development to the adult stage.

Colombani et al. observed Dilp8 in the luminal space of the wing imaginal discs, between the primary epithelia and the peripodial membrane (Colombani et al., 2012). Since the imaginal discs derive from the larval epidermis, emerging like an inflating balloon into the larval body cavity, this luminal space is topologically separated from the hemolymph by the imaginal disc epithelia (Pastor-Pareja et al., 2004). This led us to hypothesize that the imaginal disc epithelial barrier activity might regulate Dilp8 signaling by preventing access of Dilp8 in the disc lumen to the larval hemolymph, thus blocking signaling through the Lgr3 receptors in the brain and PG.

The epithelial barrier is a semi-permeable diffusion barrier between adjacent epithelial cells, and is formed by tight junctions in vertebrates and septate junctions in invertebrates (Tepass et al., 2001). Claudin proteins determine epithelial barrier exclusivity by homo- and heterodimerizing with the claudins of neighboring cells (Furuse and Tsukita, 2006). The claudins are localized to and stabilized at the junctions by a large core complex (Izumi and Furuse, 2014). However, the assembly and function of each

73 member of the septate junction complex is not well understood. One subcomplex of the
74 septate junction includes Coracle (Cora), a member of the Protein 4.1 superfamily (Fehon
75 et al., 1994), and Neurexin-IV (Nrx) (Baumgartner et al., 1996). *In vivo*, Cora and Nrx both
76 localize to the septate junctions and are necessary for stabilization of claudins at the
77 septate junction and barrier activity (Baumgartner et al., 1996; Fehon et al., 1994; Genova
78 and Fehon, 2003).
79 Here we describe experiments demonstrating that the epithelial barrier of wing
80 imaginal discs matures during the third instar in response to increasing ecdysone levels
81 and a re-localization of Coracle along the lateral membrane. This mature, prepupal
82 epithelial barrier limits Dilp8 signaling and determines the duration of the developmental
83 checkpoint after damage.
84
85 **Results**
86 <u>The activity of the Dilp8 is constrained by the imaginal disc epithelial barrier, determining</u>
87 <u>the duration of regeneration checkpoint delay</u>
88 Previously, Colombani et al. observed that Dilp8 protein could be detected in the
89 luminal space between the primary wing disc epithelia and the peripodial membrane,
90 within a region of the imaginal disc that is topologically separate from the larval
91 hemolymph (Colombani et al., 2012; Pastor-Pareja et al., 2004). We recapitulated these
92 findings by exogenously expressing a FLAG epitope-tagged allele of Dilp8 (Garelli et al.,
93 2012) in wing imaginal discs with *apterous-Gal4* (*Ap-Gal4*) to induce expression in the
94 dorsal half of the tissue (Cohen et al., 1992). We detected an accumulation of Dilp8::FLAG
95 in the lumen of the wing imaginal discs (Fig. S1). This observation led us to hypothesize
96 that this luminal localization might limit Dilp8 signaling by preventing access to Lgr3
97 receptors the brain and prothoracic gland, targets of Dilp8 to regulate growth and
98 developmental timing (Colombani et al., 2015; Garelli et al., 2015; Vallejo et al., 2015).
99 As the imaginal disc is an epithelial tissue, we examined whether disruption of the
100 epithelial barrier would produce increased developmental checkpoint signaling when
101 Dilp8 is expressed in the wing disc. To test whether the imaginal disc epithelial barrier
102 constrains Dilp8 signaling we expressed Dilp8 in the wing imaginal disc and measured
103 the effect on developmental checkpoint delay when co-expressing an RNAi construct

104 against a necessary component of the imaginal disc epithelial barrier, the claudin Kune-
105 kune (*kune*^{RNAi}, see Fig. 2A,B and S8B,C for demonstrations of RNAi activity) (Nelson et
106 al., 2010). We used *beadex-Gal4* (*Bx-Gal4*), to express either *dilp8::FLAG*, *kune*^{RNAi}, or
107 both constructs in the pouch region of the wing disc (Milán et al., 1998) and measured
108 developmental checkpoint delay relative to *lacZ* expressing control larvae. While
109 *Bx>dilp8::FLAG* and *Bx>kune*^{RNAi} expression each produce a short delay in development
110 relative to control larvae (13 and 10 hours respectively), the co-expression of Dilp8::FLAG
111 and *kune*^{RNAi}, produces a strong genetic interaction and a synergistic effect on delay (40
112 hours; Fig. 1A). To confirm this synergistic effect on delay is not due to increased activity
113 at the endogenous *dilp8* locus, we examined the effect of co-expression of Dilp8::FLAG
114 and *kune*^{RNAi} in a homozygous *dilp8* hypomorphic genetic background. Even without
115 functional endogenous copies of the *dilp8* gene, we still observe a strong genetic
116 interaction between Dilp8::FLAG and *kune*^{RNAi} and synergistic effect on developmental
117 checkpoint delay (Fig. 1B). We generated a similar synergistic interaction when we co-
118 expressed Dilp8::FLAG and an RNAi construct targeting Neurexin IV (Nrx), another
119 necessary component of the imaginal disc septate junction (Baumgartner et al., 1996)
120 (Fig. S2). These data indicate that disrupting the epithelial barrier through either of two
121 distinct genetic targets can produce synergistic extension of delay during Dilp8
122 expression. These results support the hypothesis that the epithelial barrier limits Dilp8
123 signaling from the wing imaginal disc by retaining Dilp8 in the wing disc lumen.
124
125 <u>The wing imaginal disc epithelial barrier becomes more restrictive during the last larval</u>
126 <u>instar</u>
127 The experiments above demonstrate that the wing disc epithelial barrier can limit
128 Dilp8 signaling. However, Dilp8 expression in the wing disc produces developmental
129 delay even when the wing disc epithelial barrier is not disrupted (Fig. 1A,B; Colombani et
130 al., 2012; Garelli et al., 2012). Additionally, basal levels of Dilp8 expression in the
131 developing wing disc regulate tissue symmetry through communication with Lgr3 in the
132 brain (Colombani et al., 2012; Garelli et al., 2012; Garelli et al., 2015; Vallejo et al., 2015).
133 To reconcile these observations with the sequestration of Dilp8 in the wing disc lumen
134 during in late third instar larvae, we hypothesized that there may be changes in the

135 epithelial barrier permeability during development. To examine this, we developed a
136 quantitative method for measuring epithelial barrier permeability that is an extension of a
137 method described by Lamb et al., in which the ability of fluorophore-conjugated dextran
138 to enter into the lumen of a tissue was used to assess epithelial barrier function (Lamb et
139 al., 1998). For our assay, we incubated inverted larval carcasses for 30 minutes in solution
140 containing fluorescein-conjugated dextran prior to paraformaldehyde fixation. We
141 mounted and imaged the fixed imaginal discs, then measured the fluorescein signal in
142 the lumen of the imaginal discs to quantify epithelial barrier permeability (see Materials
143 and Methods and Fig. S3 for a more complete description of this assay). When we
144 examined late third instar imaginal discs (116 hours After Egg Deposition; h AED), we
145 observed that very little fluorescent signal is detected in the wing disc lumen (Fig. 2A). To
146 determine whether exclusion of dextran from late larval wing discs is dependent on
147 epithelial barrier function, we measured fluorescence in imaginal discs that had been
148 punctured with a forceps tip prior to incubation with fluorescently-labeled dextran. As
149 expected, we observed that puncturing the wing disc led to a substantial increase in
150 luminal fluorescence detected in these discs after fixation (Fig. 2A), demonstrating that
151 an intact epithelium is necessary for the exclusion of dextran from the lumen of late third
152 instar wing discs. We then tested whether this exclusion reflected the activity of the
153 epithelial barrier by measuring dextran infiltration into wing discs expressing *kune*^{RNAi}
154 (*Ap>kune*^{RNAi}). Consistent with a critical role for the claudin Kune in wing epithelial barrier
155 function, we observed an equivalent amount of fluorescence infiltration into 116h AED
156 *Ap>kune*^{RNAi} discs as we observed in punctured discs (Fig. 2A). Therefore, loss of *kune*
157 appears to completely disrupt the epithelial barrier in late third instar wing discs.
158 To characterize the epithelial barrier exists in earlier wing discs, we examined wing
159 discs 24 hours earlier in development (92h AED, about the middle of the third and last
160 larval instar), a time when disc damage and/or Dilp8 expression is still capable of
161 producing developmental delay. In 92h AED discs we observe that physical puncture and
162 *kune*^{RNAi} expression both produce increases in dextran infiltration into the wing disc lumen
163 (Fig. 2B), similar to what we observed at 116h AED. This indicates, that wing imaginal
164 discs in the middle of the third instar have a functioning epithelial barrier mediated by
165 *kune*. However, we also noticed that the level of dextran infiltration into control 92h AED

166 wing discs appeared to be much higher than the fluorescence observed in the same
167 tissues at 116h AED (compare Fig. 2A and B), suggesting that the epithelial barrier of the
168 wing disc grows more restrictive as the larvae approach the end of the third instar. This
169 change in barrier permeability from 92h to 116h AED is also observed with 70 kD dextran
170 (Fig. S4), suggesting that the change in permeability does not reflect a change in size
171 selectivity of the barrier. To further characterize the maturation of the more restrictive
172 barrier, we used our quantitative barrier permeability assay to examine dextran infiltration
173 at six-hour intervals between 92h AED and 116h AED. We normalized the fluorescence
174 intensity to discs of equivalently staged larvae with barriers disrupted by *kune*^{RNAi}
175 expression. Consistent with our earlier observations at 92h and 116h AED, as the wing
176 disc develops, we see a progressive decrease in barrier permeability that limits the
177 infiltration of dextran into the lumen of this tissue (Fig. 2C, for an illustration of the
178 individual fluorescence distributions, see Fig. S5).
179 Based on these observations, we conclude that the wing disc epithelial barrier
180 limits diffusion throughout the third instar since we see an increase in permeability in
181 punctured or *kune*^{RNAi} expressing discs at earlier stages. However, we see a substantial
182 difference in permeability of the barrier between earlier and later discs, with the wing disc
183 epithelial barrier becoming progressively less permeable as larvae advance through the
184 third instar.
185
186 <u>Changes in epithelial barrier permeability correlate with changes in junctional protein</u>
187 <u>expression and localization</u>
188 The changes that we observe in barrier permeability during the last larval instar
189 could be due to changes in localization and/or activity of different components of the
190 epithelial barrier. To address this, we examined the localization of three major
191 components of the epithelial barrier: the claudin Kune, which forms the intercellular
192 component of the junctional barrier (Nelson et al., 2010), along with Cora and Nrx which
193 together regulate the function of pleated septate junctions in ectoderm-derived tissues
194 such as the imaginal discs (Baumgartner et al., 1996; Lamb et al., 1998). Using indirect
195 immunofluorescent staining with a Kune protein-directed antibody (Nelson et al., 2010),
196 we observed that Kune protein is localized to the apical region of the lateral membrane

197 throughout the third instar (Fig. 3D,E; Fig. S6D,E), which is the region of septate junctions
198 localization in imaginal tissues (Lamb et al., 1998; Ward IV et al., 2001). We also observed
199 that there is a substantial increase in localized Kune signal at the septate junction in late
200 third instar discs (116h AED) when compared to earlier (92h AED) discs (Fig. 3F,
201 quantification method described in Materials and Methods and diagramed in Fig. S7). To
202 localize Nrx, we used a functional Nrx-GFP fusion (Buszczak et al., 2007; Morin et al.,
203 2001). Like Kune, Nrx-GFP also localizes to the septate junctions throughout the third
204 instar and increases in signal intensity from 92 to 116 hAED (Fig. 3G-I; Fig. S6F,G). In
205 contrast to Kune and Nrx-GFP, the localization of Cora is more dynamic. At 92h AED,
206 Cora is localized either almost uniformly along the entire length lateral membrane, without
207 selectivity for the septate junction, or with slight accumulation at the septate junctions
208 (Fig. 3J,L; Fig. S6H). However, by 116h AED, Cora localization shifts to become restricted
209 to an apical-lateral localization at the septate junctions where we observe Kune and Nrx-
210 GFP signals (Fig. 3K,L; Fig. S6I).
211 In summary, we observe changes in core SJ localization that correlate with the
212 decrease in permeability of the epithelial barrier: Increased Kune localization at the
213 septate junction, and a refinement of Cora localization, from a uniform distribution along
214 the lateral membrane to localization at the apical site of the septate junction (Fig. 5G).
215
216 <u>Coracle is required to produce the changes in epithelial barrier permeability during the</u>
217 <u>last larval instar</u>
218 To determine whether Cora activity is important for the observed decrease in
219 septate junction permeability during the last larval instar, we examined the effect of
220 *cora*^{RNAi} expression on wing imaginal disc barrier permeability. At 92h AED *Ap>cora*^{RNAi}
221 expression has little impact on the wing epithelial barrier permeability. The barrier activity
222 in Cora knockdown discs is similar to control discs, with much greater selectivity than
223 *Ap>kune*^{RNAi} expressing discs, which have no functioning barrier (Fig. 4A). In contrast, in
224 late third instar wing imaginal discs (116h AED) *Ap>cora*^{RNAi} expressing discs exhibit a
225 completely disrupted epithelial barrier, comparable to that seen in *Ap>kune*^{RNAi}
226 expressing discs (Fig. 4B). Therefore, as the third instar progresses, there is a change in
227 the role of Cora for septate junction barrier activity: 92h AED wing discs have a weaker,

228 somewhat permeable, barrier activity that requires Kune, but does not depend on Cora,
229 whereas 116h AED wing discs have a more restrictive barrier activity that is completely
230 dependent on Cora.

231 Cora, Kune, and Nrx localize interdependently at the septate junctions during the
232 development of the embryonic tracheal epithelia (Nelson et al., 2010; Oshima and Fehon,
233 2011). We examined whether the same interdependence occurs in the wing imaginal disc,
234 and whether it changes during development. To do this, we visualized the localization of
235 Cora, Kune, and Nrx-GFP in discs in which we had knocked down each of these
236 components using RNAi targeting constructs driven by *Ap-Gal4*. Predictably, when we
237 expressed RNAi lines targeting Cora, Kune, and Nrx , we saw a loss of expression of the
238 targeted gene product in the dorsal compartment of both 92 and 116h AED wing discs
239 (Fig. S8), demonstrating the efficacy of the RNAi constructs. We then examined the
240 interdependence for localization of these three septate junction proteins at 92h and 116h
241 AED wing discs (Fig. 5 A-F, summarized in Fig. 5G). At 92h AED, the localization of Cora
242 along the lateral membrane is unaffected by RNAi targeted knockdown of either Kune
243 (*Ap>kune*^{RNAi}, Fig. 5A) or Nrx (*Ap>nrx*^{RNAi}, Fig. 5C). However, the localization of Cora at
244 the septate junctions at 116h AED is disrupted by RNAi targeted knockdown of either
245 Kune (*Ap>kune*^{RNAi}, Fig. 5B) or Nrx (*Ap>nrx*^{RNAi}, Fig. 5D). Therefore, the early, diffuse
246 localization of Cora along the lateral membrane does not require the activity of either
247 Kune or Nrx, but its refinement to the septate junction at the end of the larval period
248 depends on both Kune and Nrx. Nrx localization at the septate junctions in 92h AED
249 larvae is dependent on both Kune (*Ap>kune*^{RNAi}, Fig. 5A) and Cora (*Ap>cora*^{RNAi}, Fig.
250 5E). However, in the absence of Kune, we see faint Nrx localization along the lateral
251 membrane (Fig. 5A, orange arrow), which might reflect an association with Cora, whereas
252 in the absence of Cora, we see less evidence of lateral localization of Nrx (Fig. 5E,
253 arrowhead). At 116h AED, Nrx localization at the septate junction is entirely dependent
254 on both Kune and Cora (Fig. 5B,F) and no lateral redistribution of Nrx is seen in either of
255 these mutants. Finally, the septate junction localization of Kune at both 92 and 116h AED
256 is entirely dependent on Nrx (*Ap>nrx*^{RNAi}, Fig. 5C,D) and, surprisingly, Cora (*Ap>cora*^{RNAi},
257 5E,F). The requirement for Cora to localize Nrx and Kune at 92h AED is unexpected since
258 Cora is not required for the barrier activity observed at 92h AED (Fig. 4A). We address

259 some possible explanations of this observation in the Discussion section.

260 As summarized in Figure 5G, we see a complex interdependence between Kune,
261 Nrx, and Cora that determines their localization as the wing disc epithelial barrier
262 becomes more restrictive during the larval third instar. These data indicate that the
263 epithelial barrier becomes more mature and restrictive, barrier activity becomes
264 dependent on Cora as it re-localizes to the septate junctions.

265

266 <u>Ecdysone signaling promotes decreased epithelial barrier permeability and Coracle re-</u>
267 <u>localization</u>

268 The steroid hormone ecdysone is a critical endocrine regulator of *Drosophila*
269 developmental progression. During the third larval instar, pulses of ecdysone synthesis
270 drive a progressive increase in ecdysone titer throughout the larva that promotes growth
271 and differentiation of the imaginal discs (Colombani *et al.* 2005; Lavrynenko *et al.* 2015.
272 During the activation of the regenerative checkpoint following imaginal disc damage, Dilp8
273 release suppresses ecdysone synthesis through Lgr3 receptors in both the larval brain
274 and PG (Hackney et al., 2012; Halme et al., 2010; Jaszczak et al., 2016).

275 To assess whether the changes we observe in wing disc epithelial barrier
276 permeability are driven by ecdysone signaling, we first tested whether increasing
277 ecdysone titer in larvae would reduce disc barrier permeability. To do this, we transferred
278 80h larvae to either food containing 0.6 mg/ml 20-hydroxyecdysone dissolved in ethanol,
279 or food with ethanol alone as a control and assessed wing disc barrier function at 98h
280 AED using our dextran infiltration assay (illustrated Fig. S9A). In previously published
281 work we have seen that this concentration of 20-hydroxyecdysone can alter ecdysone
282 titer, but doesn't substantially accelerate pupariation timing (Colombani et al., 2005;
283 Jaszczak et al., 2015). When we assessed barrier activity in ecdysone-fed larvae, we see
284 that wing disc permeability is substantially reduced when compared with wing discs from
285 control larvae (Fig. 6A; Fig. S9B), similar to what we observe in more mature (116h AED)
286 wing discs (compare to Fig. 1C). This result indicates that increasing ecdysone titers can
287 promote the development of the restrictive barrier we see as the third larval instar
288 progresses.

289 To determine whether ecdysone acts directly on the wing disc and is necessary

290 for the change in barrier permeability, we assessed barrier function in wing discs
291 expressing the dominant-negative ecdysone receptor allele *EcR.A*^{W650A} in wing discs
292 using *Bx-Gal4*. In 92h AED discs, limiting ecdysone signaling produces little effect on
293 barrier permeability (Fig. 6B), demonstrating that the barrier function doesn't rely on
294 ecdysone signaling at this earlier stage. However, in 116h AED discs we see that blocking
295 ecdysone signaling now produces a substantial increase in epithelial barrier permeability
296 (Fig. 6C). The expression of *EcR.A*^{W650A} at 116h AED doesn't produce the same
297 disruption in barrier function as expression of *kune*^{RNAi}, rather it produces barrier
298 permeability similar to that seen in 92h AED discs (compare Figs. 6B and 6C). These
299 results demonstrate that ecdysone signaling in the wing disc is not necessary for barrier
300 activity in 92h AED wing discs, but is required for the maturation of the more restrictive
301 barrier during the third instar.
302 Since a re-localization of Cora from the lateral membrane to the apical site of the
303 septate junction is associated with the change in barrier permeability, we wanted to
304 determine whether this change in Cora localization depends on ecdysone signaling in the
305 wing disc. To do this, we examined the cellular localization of Cora in 116h AED control
306 and *EcR.A*^{W650A} wing discs. Inhibition of ecdysone signaling in the wing disc produces a
307 redistribution of Cora, from tightly localized to the apical lateral membrane, at the site of
308 the septate junction, to a more uniform distribution along the lateral membrane (compare
309 Fig. 6D and Fig. 6F; Actin staining Fig. S10), similar to what is observed in earlier 92h
310 AED discs (Fig. 3D). This re-localization of Cora is consistent with how ecdysone effects
311 the epithelial barrier, producing an increase in permeability that is similar to what is seen
312 in 92h AED wing discs, but not completely disrupting the epithelial barrier (Fig. 5A).
313 In summary, we see that the epithelial barrier activity of the wing disc at 92h AED
314 is not dependent on ecdysone signaling, whereas the re-localization of Coracle to the site
315 of the septate junction, along with the decreased permeability of the epithelial barrier, are
316 both dependent on ecdysone signaling within the wing imaginal disc epithelium.
317
318 <u>The epithelial barrier regulates the end point of regeneration</u>
319 Our data indicate that ecdysone regulates a maturation of the epithelial barrier and
320 that the epithelial barrier limits Dilp8 signaling. This led us to question whether the

321 epithelial barrier determines the duration of the regenerative checkpoint. To test this, we
322 targeted damage to the wing discs by using *Bx-Gal4* to express the TNFα homologue
323 Eiger in the pouch of the wing disc (Igaki et al., 2002; Kauppila et al., 2003; Moreno et al.,
324 2002), and examined the effects of barrier disruption on checkpoint duration. As
325 previously observed, *kune*^{RNAi} expression alone produces only a minor effect on delay,
326 whereas Eiger expression produces a substantial delay of 57 hrs. When we combine
327 Eiger and *kune*^{RNAi} expression, we see a synergistic effect on delay that is significantly
328 longer than the expected additive effect of *kune*^{RNAi} and Eiger expression alone (80 hours
329 actual, 62 hours additive; Fig. 7A). However, this additional delay is not due to increased
330 Dilp8 expression (Fig. S12), consistent with the epithelial barrier limiting Dilp8 signaling
331 at the end of the regenerative checkpoint. We observed a similar result when the epithelial
332 barrier is disrupted with *nrx*^{RNAi} (Fig. S11; Fig. S12).
333 Together, these results demonstrate that a fully-functional epithelial barrier limits
334 the duration of damage-induced checkpoint delay. Likely through the sequestration of
335 Dilp8 within the imaginal disc lumen.
336
337 **Discussion**
338 <u>How is the end of regeneration determined?</u>
339 Despite progress towards understanding the cues that initiate regeneration and
340 the signaling pathways that contribute to regenerative growth and repatterning, the
341 mechanisms for determining when the target of regeneration is reached remain poorly
342 understood (Fox et al., 2020). Here, we demonstrate that the formation of a functional,
343 mature epithelial barrier determines the duration of the regenerative period by regulating
344 Dilp8 signaling. Since Dilp8 is seen in the imaginal disc lumen (Colombani et al., 2012;
345 Fig. S1), it seems likely that the epithelial barrier limits Dilp8 signaling by physically
346 sequestering Dilp8 protein in the lumen of the imaginal disc, separated from the
347 hemolymph and access to the prothoracic gland and the brain, where Dilp8 acts through
348 Lgr3 to inhibit ecdysone production (Colombani et al., 2012; Colombani et al., 2015;
349 Garelli et al., 2012; Garelli et al., 2015; Jaszczak et al., 2016). Therefore, we propose that
350 as regeneration is completed, the balance between Dilp8 signaling (which delays
351 developmental progression and limits ecdysone synthesis) and ecdysone signaling

352 (which shuts down regenerative activity and promotes the advancement from the larval
353 to the pupal phase of development) is shifted to favor ecdysone signaling by the
354 establishment of the mature, prepupal epithelial barrier which traps Dilp8 in the
355 regenerated disc lumen. In this way, the re-establishment of a restrictive epithelial barrier
356 would be one mechanism for epithelial tissues to communicate their functional restoration
357 and the completion of regeneration (model, Fig. 7B).
358
359 Regulated maturation of the epithelial barrier
360 In these experiments, we also demonstrate that the function of the epithelial barrier
361 changes during the third instar, growing more restrictive prior to pupariation in response
362 to ecdysone. Although we were unable to determine the direct target of EcR that produces
363 this change in barrier activity, we observe that ecdysone triggers the re-localization of
364 Cora from a pattern of diffuse localization along the length of the lateral membrane to a
365 specific localization at the septate junctions in the apical lateral membrane. This re-
366 localization correlates with the establishment of a mature, restrictive epithelial barrier.
367 This mechanism is similar to observations that Cora re-localizes to the septate junctions
368 during the embryonic stages 12 and 17 in the developing salivary gland and embryonic
369 epidermis, which is when the epithelial barrier is established in these tissues (Hall and
370 Ward, 2016; Oshima and Fehon, 2011; Paul et al., 2003). Similar to the end of larval
371 development, there is a peak of ecdysone production during this embryonic period and
372 EcR is expressed in both these maturing epithelia (Kozlova and Thummel, 2000; Kozlova
373 and Thummel, 2003; Tan et al., 2014). This leads us to suggest that the regulation of
374 Cora localization by ecdysone may be a general mechanism for the maturation of a
375 restrictive barrier in developing *Drosophila* epithelia.
376 However, our examination of epithelia barrier maturation in the wing disc also
377 raises some interesting questions about the role of individual septate junction
378 components which remain to be answered. In particular, the role is of the core
379 components Cora and Kune in barrier function earlier in the third instar, at 92h AED. The
380 barrier at this time is not as restrictive as is observed later, but still limits the passage of
381 10kD dextran molecules (Fig. 2B, compare Intact to Punctured). Kune is required for this
382 early barrier activity but Cora is not necessary (Fig. 4). However, when we block Cora

383 expression with an RNAi, we see that Cora is necessary for the localization of both Nrx
384 and Kune at both 92h and 116h AED (Fig. 5). This suggests that in Cora mutant tissues
385 at 92h AED, the mis-localized Kune (and Nrx) still retain some residual barrier activity,
386 which is lost at 116h AED. One possible explanation is that a low level of Nrx and Kune
387 localization along the lateral membrane may remain in Cora mutant tissues, but was
388 undetectable by our imaging. This low level of Nrx and Kune localization may be sufficient
389 to support early barrier activity in early discs, but not a similar barrier activity at the end
390 of the third instar. Further study will be necessary to better understand how each of these
391 core components contribute to the barrier as the wing disc matures.
392
393 Could other signaling pathways be regulated by epithelial barrier maturation?
394 Our observation that Dilp8 is constrained by the wing disc epithelial barrier raises
395 the question of whether other signals are regulated by sequestration in the imaginal disc
396 lumen. One interesting possibility is the morphogen Decapentaplegic (Dpp, *Drosophila*
397 BMP2/4 ortholog). Dpp has numerous, critical roles in growth and patterning across
398 development, including in imaginal discs (Hamaratoglu et al., 2014). Setiawan et al.
399 showed that during larval development, Dpp produced in the imaginal tissues inhibits
400 ecdysone production in the prothoracic gland early in the third larval instar. By the late
401 third instar, Dpp can no longer be detected in the larval hemolymph and the Dpp activity
402 in the prothoracic gland ceases, despite high levels of Dpp expression in imaginal discs.
403 Setiawan et al. hypothesized that this was due in part to the dilution of circulating Dpp as
404 a result of increased hemolymph volume and the trapping of Dpp in imaginal disc tissues,
405 but were unable to identify how the tissues trapped Dpp (Setiawan et al., 2018). Our data
406 suggest that Dpp might be trapped in late third instar discs by the maturing epithelial
407 barrier. Further experiments will be necessary to test this hypothesis.
408 In summary, our data demonstrate that in *Drosophila*, ecdysone signaling alters
409 the permeability of the wing disc epithelial barrier during the third and final larval instar.
410 We also show that mature, restrictive wing disc epithelial barrier limits Dilp8 signaling,
411 determining the duration of the regenerative checkpoint. This provides an interesting
412 mechanism by which the barrier, as a primary characteristic of epithelial tissues, can
413 report the successful completion of regeneration.

414

415 **Materials and Methods**

416 Drosophila stocks and husbandry

417 The fly stocks used were, or were generated from crosses with, Ap-Gal4; UAS-
418 LacZ.NZ, UAS-Dcr2/ SM6-TM6B (derived from Bloomington 3041), Bx-Gal4, UAS-Dcr2
419 (Dr. David Bilder), UAS-LacZ.NZ (BL3955), UAS-Kune[RNAi] (VDRC GD3962), UAS-
420 NrxIV[RNAi] (VDRC GD8353), UAS-Sinu[RNAi] (VDRC GD44928), UAS-Cora[RNAi]
421 (Bloomington 51845), UAS-EcR.A.W650A (Bloomington 9451), NrxIV-GFP (Bloomington
422 50798), UAS-eiger, UAS-Dilp8::3xFLAG (Dr. Maria Dominguez) (Garelli et al., 2012), and
423 Dilp8::GFP (Bloomington 33079).

424 Stocks and crosses were maintained in 25° incubators with a 12-hour alternating
425 light-dark cycle. Developmental timing was synchronized through egg staging, with
426 collection from a 4-hour egg-laying interval on grape agar plates (Genesee Scientific) with
427 a small amount of baker's yeast paste. At 24h AED, 20-30 first instar larvae were
428 transferred into vials containing cornmeal-yeast-molasses media (Archon Scientific
429 B101). Ecdysone food was prepared by dissolving 1.2 mg 20-hydroxyecdysone (Sigma)
430 dissolved in 95% ethanol in 2 mL of food media (final concentration 0.6 mg/mL), or an
431 equivalent volume of ethanol for control. Larvae were reared as previously described until
432 80h AED then transferred to the ecdysone or ethanol-control food, approximately 6 larvae
433 per vial (Halme et al., 2010).

434 For specific genotypes used in each Figure see Supplementary Materials and
435 Methods.

436

437 Dissection and Immunofluorescent Staining

438 Larvae were inverted and cleaned in PBS then fixed with 4% paraformaldehyde in
439 PBS (20 min) and washed with PBS (twice for 5 min each). The tissues were
440 permeabilized with 0.3% Triton in PBS (twice for 10 min each) then washed with a
441 blocking solution of 10% goat and 0.1% Triton in PBS (30 min). Then the tissues were
442 incubated rocking in primary antibody solutions (overnight at 4° or for two-to-four hours
443 at room temperature). The process was repeated for secondary antibodies and then the
444 tissues were incubated rocking in 80% glycerol in PBS (overnight at 4°). The tissues were

445 stored at 4° in 80% glycerol and were mounted for imaging within one week of staining.
446 Imaginal discs were isolated from the stained tissues and mounted on glass slides with
447 Vectashield (Vector Laboratories). Cross-section images were taken from tissues
448 mounted on slides with the coverslips raised by double-sided tape. For experiments with
449 Kune or FLAG staining, the above procedure modified to reduce non-specific staining. In
450 these experiments, larvae were dissected in Schneider's Insect Medium (Sigma-Aldrich),
451 fixed in 4% paraformaldehyde in Schneider's Insect Medium (Sigma-Aldrich), stained in
452 one day within three days of dissection, and imaged within three days of staining.
453 Antibody solutions were prepared in 10% goat serum and 0.1% Trion in PBS. The
454 primary antibodies that were used are mouse β-Gal (1:250; Promega), mouse anti-Cora
455 C615.16 (1:400; Developmental Studies Hybridoma Bank), mouse anti-FLAG M2 F1804
456 (1:250; Sigma-Aldrich), rabbit β-Gal (1:400; MP), and rabbit anti-Kune (1:1000; Dr. Mikio
457 Furuse; Nelson et al., 2010). The secondary antibodies that were used are goat anti-
458 mouse or anti-rabbit Alexa405, Alexa488, or Alexa633 (1:1000; ThermoFisher). F-actin
459 was identified by Rhodamine-conjugated Phallodin (1:100; ThermoFisher) staining that
460 was performed concurrently with secondary antibody incubations.
461
462 Imaging and Statistical Analysis
463 Confocal imaging was done using an Olympus FluoView 1000 1000 (Figures 2AB,
464 3FIL, 6BCDEF, S3, S4, S10) within the University of Virginia Department of Cell Biology
465 or a Zeiss LSM 700 (Figures 2C, 3, 4, 5, 6ABC, S1, S5, S6, S7, S8, S9, S12) in the
466 University of Virginia Advanced Microscopy Facility (RRID:SCR_018736). Laser power
467 and gain settings for each set of stained samples were based on the experimental group
468 with the highest fluorescence intensity in each channel, and kept constant within the
469 experiment. To compare between independently repeated experiments, we normalized
470 within the experiment as indicated. Images were processed and quantified with
471 Fiji/ImageJ (Schindelin et al., 2012).
472 Prism 8 software was used for Statistical Analysis. The specific tests that were
473 used are listed in the figure descriptions.
474
475 Dextran Assay

476 Larvae were inverted and cleaned in Schneider's Insect Medium (Sigma-Aldrich)
477 then transferred into a 1:8 dilution of 10 kD fluorescein conjugated dextran (Invitrogen) in
478 Schneider's Insect Medium (Sigma-Aldrich) and incubated rocking and covered at room
479 temperature for 30 minutes. The tissues were washed briefly (approximately 1 minute) in
480 Schneider's Insect Medium (Sigma-Aldrich) to remove excess dextran, then fixed with 4%
481 paraformaldehyde in Schnider's Insect Media. Tissues were washed, stained, and
482 imaged as previously described.
483 Fluorescent dextran infiltration was measured using Fiji/ImageJ (Schindelin et al.,
484 2012), taking the mean intensity along a line in the imaginal disc lumen (identified by
485 rhodamine phalloidin or Cora staining) and subtracting background from outside the disc
486 area. Discs that appeared punctured were either not measured or categorized separately
487 from intact discs. The fluorescence intensity varies with each experiment, so the data
488 were normalized to the mean from controls that were incubated simultaneously.
489
490 Quantification of septate junction component localization
491 Septate junction localization was quantified using Fiji/ImageJ (Schindelin et al.,
492 2012). Two lines were drawn to collect fluorescence intensity of the junctions, the first
493 across the apical-lateral surface of cells near the center of where the septate junctions
494 were localized, and the second along the middle of the cells. Junctional intensity, or
495 membrane intensity for the medial region, was considered as an average of the 7 pixels
496 surrounding local maxima. In this way we hoped to average out misrepresentations in the
497 data that arose from slices that cut through cells approximately parallel to the cell
498 membranes and from slices that cut through tricellular junctions and had more protein
499 from the third cell. None of the proteins we looked at are reported or appeared to have
500 specific tricellular activity. We then took the ratio of the average junctional peak intensity
501 to the average medial peak intensity (Fig. S7).
502 Peak identification was adjusted in three steps to reduce false identification of a
503 membrane peak due to the noise within an image, especially with regards to Anti-Kune
504 and Anti-Cora staining. First, to ensure the peak wasn't a result of a slightly brighter
505 random pixel, we removed peaks that were below the median fluorescence of the entire
506 line. Second, to ensure the identified peak was localized at the membrane, we removed

507 points of Anti-Kune and Anti-Cora staining that did not have a Nrx::GFP peak within the
508 same 7-pixel range. We used Nrx::GFP instead of Actin (Rhodamine Phallodin) staining
509 for this because Nrx::GFP has extremely low noise as it is a membrane bound GFP
510 produced within the cell and does not need to be stained for. Nrx::GFP also has a very
511 high association with the membrane even away from canonical apical-lateral staining,
512 while this fluorescence is very dim, it is still detectable and highly correlated with the
513 membrane. Finally, to ensure that we took a measurement at the membrane and not at a
514 noisy region within the cell, if no Anti-Kune or Anti-Cora peak was identified within the 7-
515 pixel range of the Nrx::GFP peak, a measurement was added at the same placement of
516 the Nrx::GFP peak. Together these adjustments reduced the number of peak
517 identifications in each image by approximately 1-10 junctions depending on the stain
518 (most images had 40-60 junctions following adjustments).
519

520 **Acknowledgements**
521 The authors would like to acknowledge Dr. David Bilder, Dr. Pierre Leopold, Dr. Maria
522 Dominguez, Dr. Mikio Furuse, and Dr. Robert Ward for reagents and/or *Drosophila* stocks
523 critical for the completion of these experiments. The authors would like to acknowledge
524 the University of Virginia Advanced Microscopy Facility (RRID:SCR_018736) for training
525 and access to the LSM700 confocal microscope.
526

527 **Competing interests**
528 No competing interests are declared
529

530 **Funding**
531 This work was supported by the National Institutes of Health (GM099803 to A.H.,
532 GM008136 to D.D., and GM008715 to F.K.) and the March of Dimes (5FY1260 to A.H.)
533

534 **Data availability**
535 There are no publicly available datasets associated with this work. All data underlying
536 this work will be made available to researchers upon request.
537

538 **References**

539 Baumgartner, S., Littleton, J. T., Broadie, K., Bhat, M. a., Harbecke, R., Lengyel, J. a.,
540 Chiquet-Ehrismann, R., Prokop, A. and Bellen, H. J. (1996). A Drosophila
541 neurexin is required for septate junction and blood-nerve barrier formation and
542 function. *Cell* 87, 1059–1068.

543 Buszczak, M., Paterno, S., Lighthouse, D., Bachman, J., Planck, J., Owen, S., Skora, A.
544 D., Nystul, T. G., Ohlstein, B., Allen, A., et al. (2007). The carnegie protein trap
545 library: A versatile tool for drosophila developmental studies. *Genetics* 175,
546 1505–1531.

547 Cohen, B., McGuffin, M. E., Pfeifle, C., Segal, D. and Cohen, S. M. (1992). apterous, a
548 gene required for imaginal disc development in Drosophila encodes a member of
549 the LIM family of developmental regulatory proteins. *Genes and Development* 6,
550 715–729.

551 Colombani, J., Bianchini, L., Layalle, S., Pondeville, E., Dauphin-Villemant, C.,
552 Antoniewski, C., Carré, C., Noselli, S. and Léopold, P. (2005). Antagonistic
553 actions of ecdysone and insulins determine final size in Drosophila. *Science* 310,
554 667–670.

555 Colombani, J., Andersen, D. S. and Leopold, P. (2012). Secreted Peptide Dilp8
556 Coordinates Drosophila Tissue Growth with Developmental Timing. *Science* 336,
557 582–585.

558 Colombani, J., Andersen, D. S., Boulan, L., Boone, E., Romero, N., Virolle, V., Texada,
559 M. and Léopold, P. (2015). Drosophila Lgr3 Couples Organ Growth with
560 Maturation and Ensures Developmental Stability. *Current biology : CB* 25, 2723–
561 9.

562 Fehon, R. G., Dawson, I. a and Artavanis-Tsakonas, S. (1994). A Drosophila
563 homologue of membrane-skeleton protein 4.1 is associated with septate
564 junctions and is encoded by the coracle gene. *Development (Cambridge,*
565 *England)* 120, 545–557.

566 Fox, D. T., Cohen, E. and Smith-Bolton, R. (2020). Model systems for regeneration:
567 Drosophila. *Development* 147,.

568 Furuse, M. and Tsukita, S. (2006). Claudins in occluding junctions of humans and flies.
569 *Trends in cell biology* 16, 181–8.
570 Garelli, a., Gontijo, a. M., Miguela, V., Caparros, E. and Dominguez, M. (2012).
571 Imaginal Discs Secrete Insulin-Like Peptide 8 to Mediate Plasticity of Growth and
572 Maturation. *Science* 336, 579–582.
573 Garelli, A., Heredia, F., Casimiro, A. P., Macedo, A., Nunes, C., Garcez, M., Mantas
574 Dias, A. R., Volonte, Y. A., Uhlmann, T., Caparros, E., et al. (2015). ARTICLE
575 Dilp8 requires the neuronal relaxin receptor Lgr3 to couple growth to
576 developmental timing.
577 Genova, J. L. and Fehon, R. G. (2003). Neuroglian, Gliotactin, and the Na+/k+ ATPase
578 are essential for septate junction function in Drosophila. *Journal of Cell Biology*
579 161, 979–989.
580 Hackney, J. F. and Cherbas, P. (2014). Injury response checkpoint and developmental
581 timing in insects. *Fly* 8, 226–231.
582 Hackney, J. F., Zolali-Meybodi, O. and Cherbas, P. (2012). Tissue damage disrupts
583 developmental progression and ecdysteroid biosynthesis in Drosophila. *PloS one*
584 7, e49105.
585 Hall, S. and Ward, R. E. (2016). Septate Junction Proteins Play Essential Roles in
586 Morphogenesis Throughout Embryonic Development in Drosophila. *G3*
587 *(Bethesda, Md.)* 6, 2375–84.
588 Halme, A., Cheng, M. and Hariharan, I. K. (2010). Retinoids Regulate a Developmental
589 Checkpoint for Tissue Regeneration in Drosophila. *Current Biology* 20, 458–463.
590 Hamaratoglu, F., Affolter, M. and Pyrowolakis, G. (2014). Dpp/BMP signaling in flies:
591 From molecules to biology. *Seminars in Cell & Developmental Biology* 32, 128–
592 136.
593 Igaki, T., Kanda, H., Yamamoto-Goto, Y., Kanuka, H., Kuranaga, E., Aigaki, T. and
594 Miura, M. (2002). Eiger, a TNF superfamily ligand that triggers the Drosophila
595 JNK pathway. *EMBO Journal* 21, 3009–3018.
596 Izumi, Y. and Furuse, M. (2014). Molecular organization and function of invertebrate
597 occluding junctions. *Seminars in Cell & Developmental Biology* 36, 186–193.

598 Jaszczak, J. S., Wolpe, J. B., Dao, A. Q. and Halme, A. (2015). Nitric oxide synthase
599 regulates growth coordination during Drosophila melanogaster imaginal disc
600 regeneration. *Genetics* 200, 1219–1228.
601 Jaszczak, J. S., Wolpe, J. B., Bhandari, R., Jaszczak, R. G. and Halme, A. (2016).
602 Growth Coordination During Drosophila melanogaster Imaginal Disc
603 Regeneration Is Mediated by Signaling Through the Relaxin Receptor Lgr3 in the
604 Prothoracic Gland. *Genetics* 204, 703–709.
605 Kauppila, S., Maaty, W. S. A., Chen, P., Tomar, R. S., Eby, M. T., Chapo, J., Chew, S.,
606 Rathore, N., Zachariah, S., Sinha, S. K., et al. (2003). Eiger and its receptor,
607 Wengen, comprise a TNF-like system in Drosophila. *Oncogene* 22, 4860–4867.
608 Kozlova, T. and Thummel, C. S. (2000). Steroid Regulation of Postembryonic
609 Development and Reproduction in Drosophila. *Trends in Endocrinology &*
610 *Metabolism* 11, 276–280.
611 Kozlova, T. and Thummel, C. S. (2003). Essential Roles for Ecdysone Signaling During
612 Drosophila Mid-Embryonic Development. *Science* 301, 1911–1914.
613 Lamb, R. S., Ward, R. E., Schweizer, L. and Fehon, R. G. (1998). Drosophila coracle, a
614 member of the protein 4.1 superfamily, has essential structural functions in the
615 septate junctions and developmental functions in embryonic and adult epithelial
616 cells. *Molecular biology of the cell* 9, 3505–3519.
617 Milán, M., Diaz-Benjumea, F. J. and Cohen, S. M. (1998). Beadex encodes an LMO
618 protein that regulates Apterous LIM-homeodomain activity in Drosophila wing
619 development: A model for LMO oncogene function. *Genes and Development* 12,
620 2912–2920.
621 Moreno, E., Yan, M. and Basler, K. (2002). Evolution of TNF signaling mechanisms:
622 JNK-dependent apoptosis triggered by Eiger, the Drosophila homolog of the TNF
623 superfamily. *Current Biology* 12, 1263–1268.
624 Morin, X., Daneman, R., Zavortink, M. and Chia, W. (2001). A protein trap strategy to
625 detect GFP-tagged proteins expressed from their endogenous loci in Drosophila.
626 *Proceedings of the National Academy of Sciences of the United States of*
627 *America* 98, 15050–15055.

628 Nelson, K. S., Furuse, M. and Beitel, G. J. (2010). The Drosophila Claudin Kune-kune is
629 required for septate junction organization and tracheal tube size control. *Genetics*
630 185, 831–9.
631 Oshima, K. and Fehon, R. G. (2011). Analysis of protein dynamics within the septate
632 junction reveals a highly stable core protein complex that does not include the
633 basolateral polarity protein Discs large. *Journal of Cell Science* 124, 2861–2871.
634 Pastor-Pareja, J. C., Grawe, F., Martín-Blanco, E. and García-Bellido, A. (2004).
635 Invasive cell behavior during Drosophila imaginal disc eversion is mediated by
636 the JNK signaling cascade. *Developmental Cell* 7, 387–399.
637 Paul, S. M., Ternet, M., Salvaterra, P. M. and Beitel, G. J. (2003). The Na+/K+ ATPase
638 is required for septate junction function and epithelial tube-size control in the
639 Drosophila tracheal system. *Development (Cambridge, England)* 130, 4963–
640 4974.
641 Schindelin, J., Arganda-Carreras, I., Frise, E., Kaynig, V., Longair, M., Pietzsch, T.,
642 Preibisch, S., Rueden, C., Saalfeld, S., Schmid, B., et al. (2012). Fiji: an open-
643 source platform for biological-image analysis. *Nature Methods* 9, 676–682.
644 Setiawan, L., Pan, X., Woods, A. L., O'connor, M. B. and Hariharan, I. K. (2018). The
645 BMP2/4 ortholog Dpp can function as an inter-organ signal that regulates
646 developmental timing.
647 Tan, K. L., Vlisidou, I. and Wood, W. (2014). Ecdysone Mediates the Development of
648 Immunity in the Drosophila Embryo. *Current Biology* 24, 1145–1152.
649 Tepass, U., Tanentzapf, G., Ward, R. and Fehon, R. (2001). *EPITHELIAL CELL*
650 *POLARITY AND CELL JUNCTIONS IN DROSOPHILA*.
651 Vallejo, D. M., Juarez-Carreño, S., Bolivar, J., Morante, J. and Dominguez, M. (2015). A
652 brain circuit that synchronizes growth and maturation revealed through Dilp8
653 binding to Lgr3. *Science (New York, N.Y.)* 1–16.
654 Ward IV, R. E., Schweizer, L., Lamb, R. S. and Fehon, R. G. (2001). The protein 4.1,
655 ezrin, radixin, moesin (FERM) domain of drosophila coracle, a cytoplasmic
656 component of the septate junction, provides functions essential for embryonic
657 development and imaginal cell proliferation. *Genetics* 159, 219–228.
658

659 **Figures and Figure Legends**

660

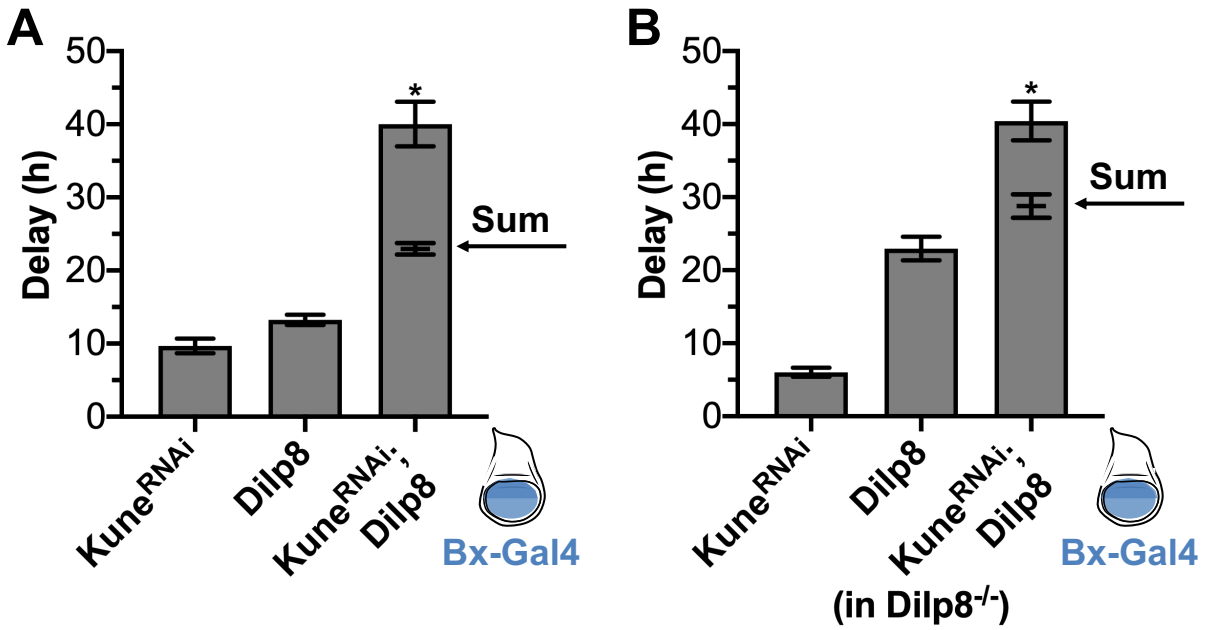

661

662 **Figure 1.** The epithelial barrier limits Dilp8 signaling. (A) Co-expression of *kune*^{RNAi} and
663 Dilp8 induces synergistic delay. Ectopic expression of either *kune*^{RNAi}, Dilp8, or co-
664 expression of *kune*^{RNAi} and Dilp8 (*kune*^{RNAi}; Dilp8) induce developmental delay compared
665 to LacZ controls when expressed in the wing imaginal disc under Bx-Gal4 (expression
666 region in blue). The delay induced by co-expression of *kune*^{RNAi} and Dilp8 (*kune*^{RNAi};
667 Dilp8) is significantly more than the sum of the delay induced by *kune*^{RNAi} and Dilp8
668 expressed alone (sum indicated by arrow). (B) This trend holds true when endogenous
669 Dilp8 is limited by expression in a Dilp8 hypomorphic background
670 (Dilp8^{MI00727}/Dilp8^{MI00727}; Garelli et al., 2012). Data were collected from at least three
671 independent experiments, bars represent mean ± SEM, * $p < 0.05$ from one sample t-test
672 comparing the additive value and observed delay.

673

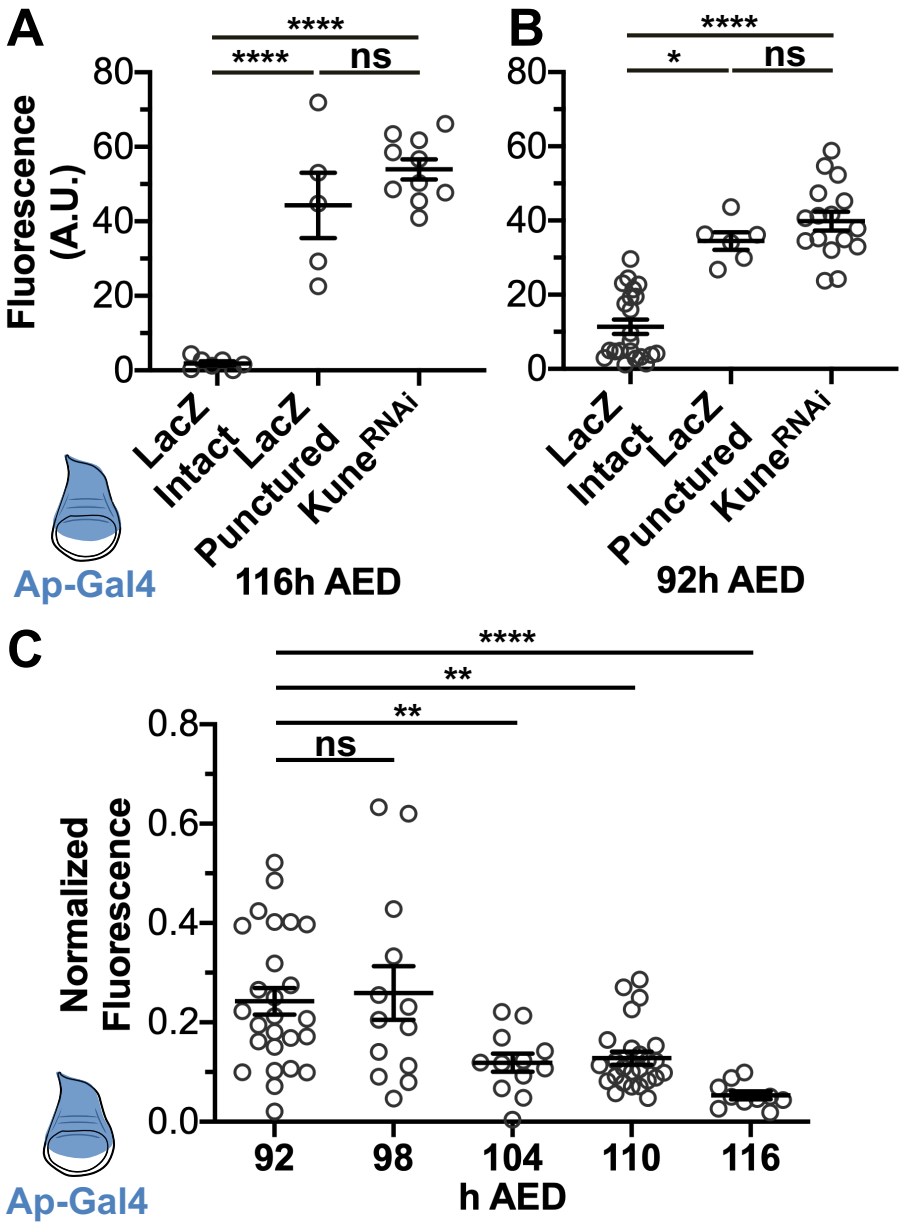

674

675 **Figure 2.** The wing disc epithelial barrier becomes more restrictive with progression
676 through the third larval instar. (A-B) The wing imaginal disc epithelial barrier excludes 10
677 kD dextran and the function of the barrier is dependent on Kune at both (A) 116h and (B)
678 92h AED. LacZ and Kune^{RNAi} were expressed in the imaginal disc with Ap-Gal4
679 (expression area diagramed in blue). Imaginal discs were incubated in 10 kD fluorescein-
680 conjugated dextran for 30 minutes prior to (see methods for details). Luminal intensity
681 was measured in the LacZ controls, LacZ controls that were punctured during dissection
682 prior to fixing, and the Kune^{RNAi} expressing discs. (C) The maturation of the epithelial

683 barrier occurs gradually from 92h to 116h AED. Every 6 hours from 92h and 116h AED,
684 barrier function was measured, as previously described, in wing imaginal discs
685 expressing LacZ or Kune^{RNAi} with Ap-Gal4. Data indicate luminal intensity of intact LacZ
686 expressing discs normalized to the mean luminal intensity of the Kune^{RNAi} expressing
687 discs from the same timepoint, Kune^{RNAi} data represented in Figure S6. (A-C) Graphs
688 represent mean ± SEM, with individual points indicating values of single images. Left to
689 right, n = (A) 7, 5, 10, (B) 22, 6, 16, (C) 26, 13, 12, 25, 10. (A-C) ns not significant, * $p <$
690 0.05, ** $p < 0.01$, **** $p < 0.0001$ as calculated by (A,C) Brown-Forsythe and Welch
691 ANOVA with Dunnett's T3 test for multiple comparisons or (B) one-way ANOVA with
692 Tukey test for multiple comparisons.
693

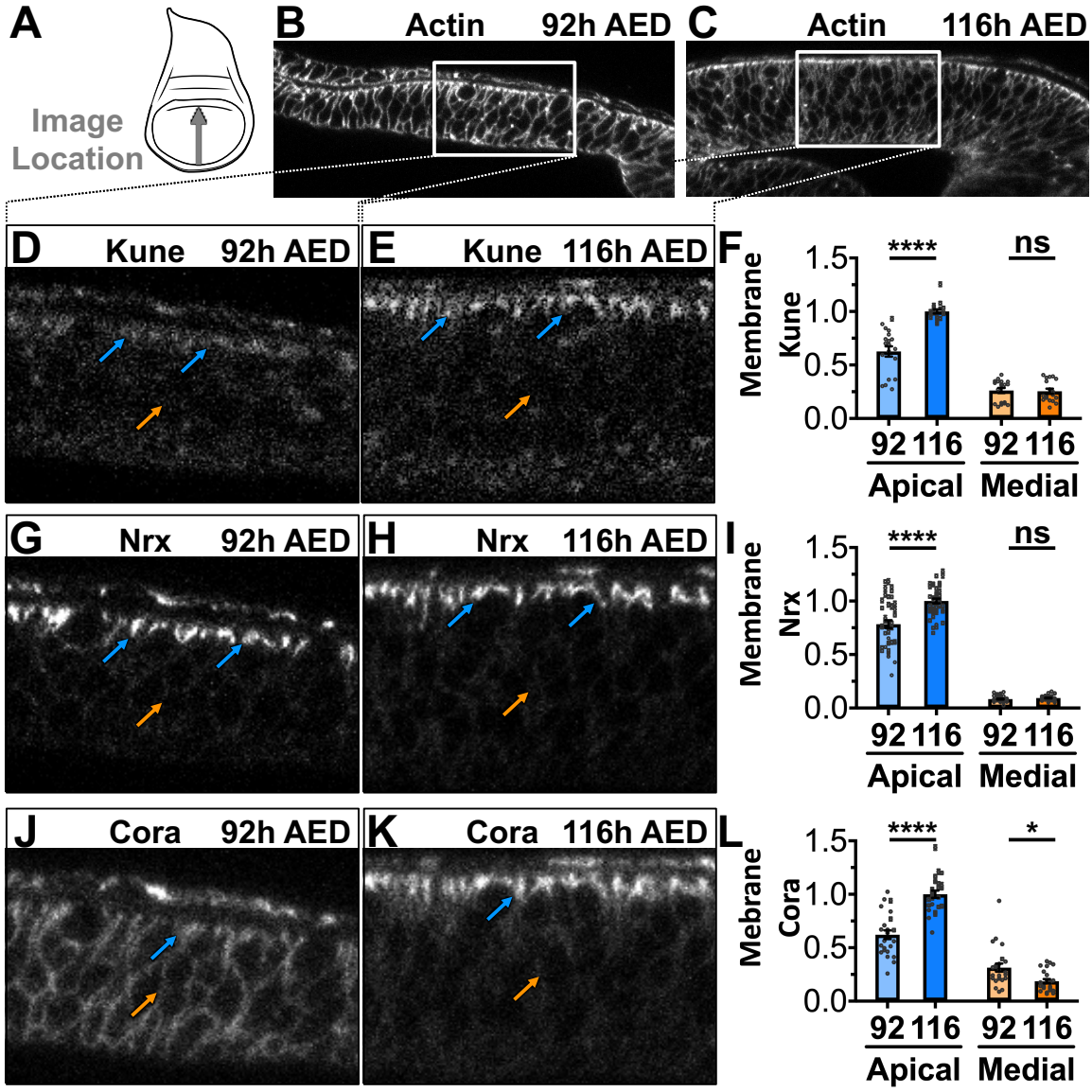

Figure 3. The localization of septate junction components changes between 92h and 116h AED. (A) Cross sections of the pouch region of the wing imaginal discs were collected by capturing X-Z images. All images were similarly oriented with the ventral portion of the disc facing left and the dorsal portion of the disc facing right. Approximate region and direction of the images is indicated. (B-C) Disc area was determined by Actin (rhodamine phalloidin) staining at (B) 92h and (C) 116h AED. The box represents the area of focus for images in D, G and J for the 92h AED disc and E, H, and K for the 116h AED disc. Blue arrows indicate apical-lateral localization, orange arrows indicate medial-lateral localization (or lack thereof). (D-E) Representative images of Kune localization at (D) 92h and (E) 116h AED showing of apical-lateral Kune localization. (F) Quantification

705 of Kune localized along the apical-lateral and medial-lateral membrane, normalized to
706 mean Kune membrane intensity at 116h AED. (G-H) Representative images of Nrx
707 localization at 92h (G) and 116h (H) AED showing apical-lateral localization. (I)
708 Quantification of Nrx localized along the apical-lateral and medial-lateral membrane,
709 normalized to mean Nrx membrane intensity at 116h AED. (J-K) Representative images
710 of Cora localization at (J) 92h and (K) 116h AED showing diffuse Cora localization at 92h
711 AED, and apical-lateral Cora localization at 116h AED. (L) Quantification of Cora localized
712 along the apical-lateral and medial-lateral membrane, normalized to mean Cora
713 membrane intensity at 116h AED. (D,E,G,H,J,K) Full images in Figure S6. (F,I,L)
714 Individual points represent mean ± SEM for each image, with the n considered to be the
715 number of cell-cell interactions across the region measured. Bars represent mean ± SEM
716 across the images, with the n considered to be the number of images measured. Details
717 about the quantification method are explained in the Methods Section and Figure S7. n =
718 (F) 19, 92h AED and 18, 116h AED images, (I) 39, 92h AED and 41, 116h AED images,
719 and (L) 24, 92h AED and 24, 116h AED images. ns not significant, * $p < 0.05$, **** $p <$
720 0.0001 as calculated by unpaired, two-tailed t-test, except for apical-lateral Kune, which
721 had unequal variance, in this case significance was calculated by unpaired, two-tailed t-
722 test with Welch's correction.
723
724

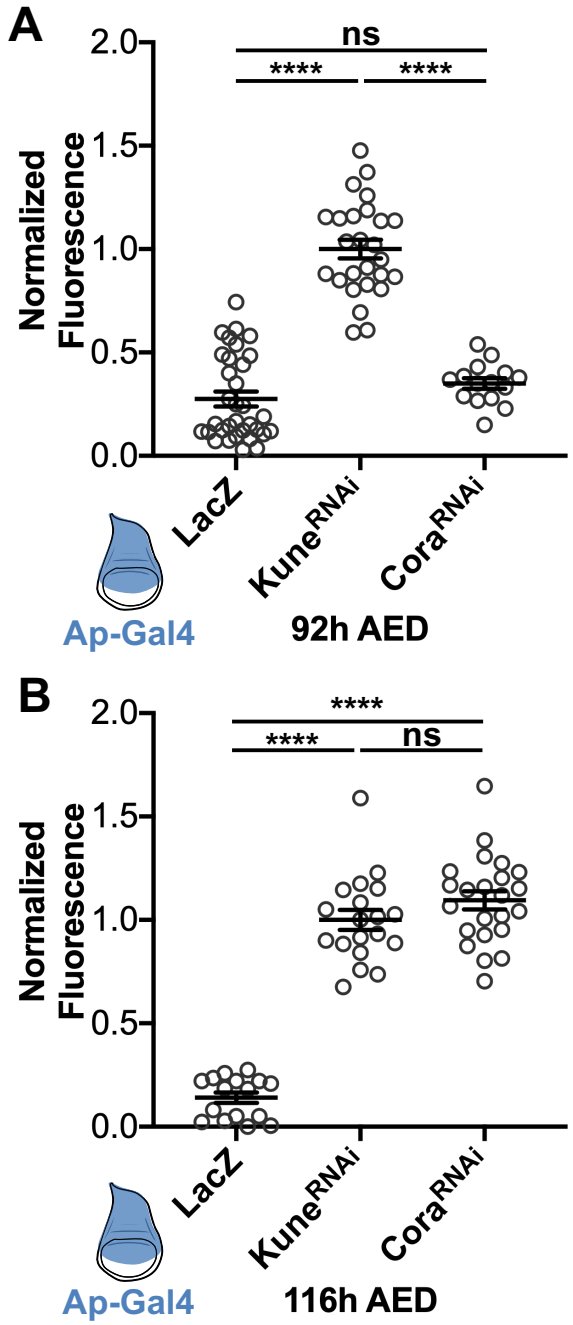

Figure 4. The role of Cora in epithelial barrier activity changes from 92h and 116h AED. (A-B) Function of the epithelial barrier in discs expressing *lacZ*, *kune*^{RNAi}, or *cora*^{RNAi} (using Ap-Gal4, expression diagramed in blue) to exclude 10 kD dextran at (A) 92h and (B) 116h AED. At 92h AED, the barrier of *cora*^{RNAi} expressing discs is similar to *lacZ* expressing discs. At 116h AED, the barrier of *cora*^{RNAi} expressing discs is similar to *kune*^{RNAi} expressing discs. Data are normalized to the mean luminal intensity of *kune*^{RNAi}

732 expressing discs. Graph represents mean ± SEM, with individual points indicating values
733 of single images. Left to right, n = (A) 33, 26, and 15 images, and (B) 16, 19, and 23
734 images. ns not significant, **** $p < 0.0001$ as calculated by Brown-Forsythe and Welch
735 ANOVA with Dunnett's T3 test for multiple comparisons.
736

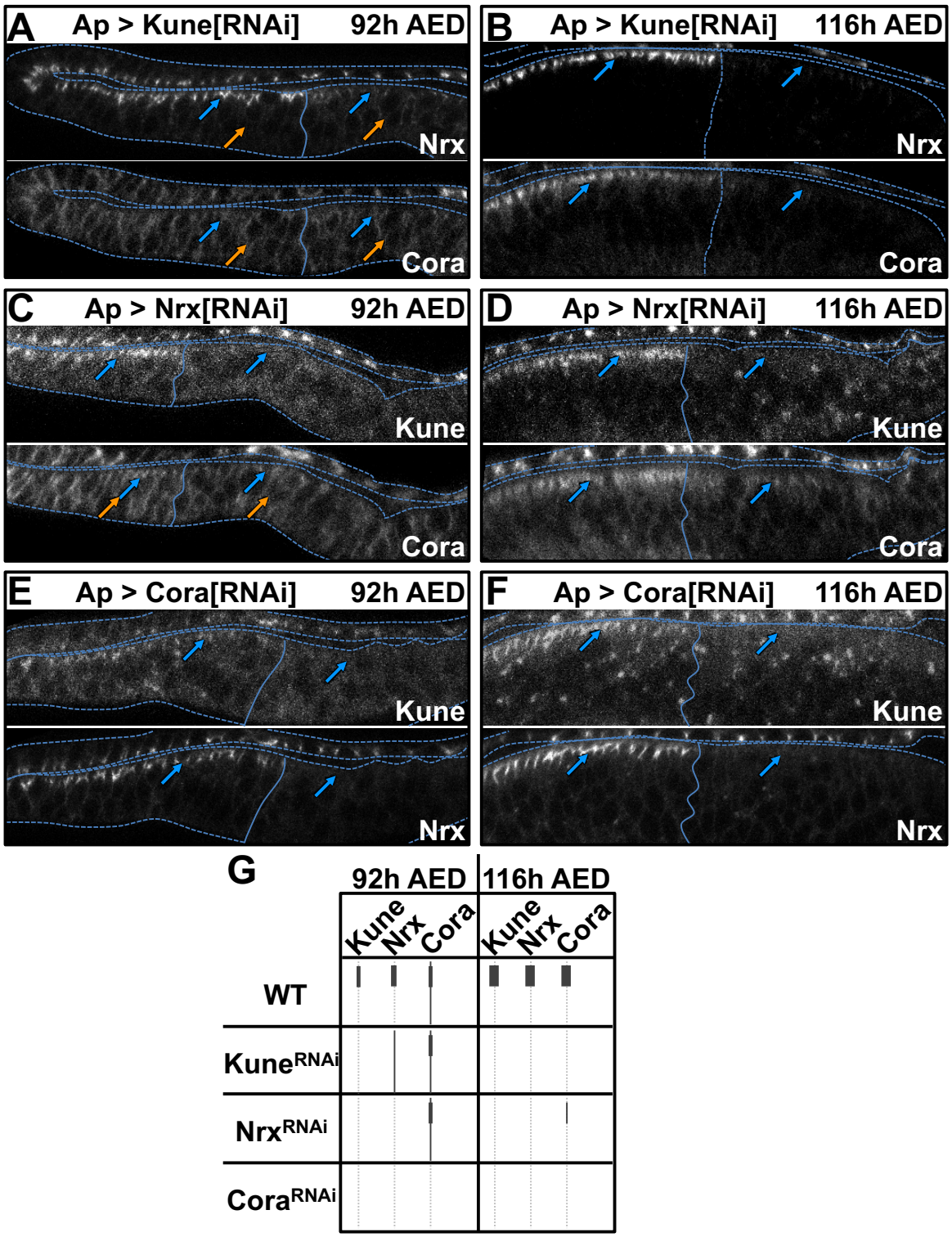

Figure 5. The localization of Nrx and Kune is dependent on Cora at both 92h and 116h AED. Ap-Gal4 was used to express *kune*^{RNAi}, *nrx*^{RNAi}, or *cora*^{RNAi} and the localization of the Kune, Nrx, and Cora were assessed (images with same protein as the RNAi are in

741 Figure S8). Images were taken spanning the dorsal-ventral boundary (solid line, defined
742 by data in Figure S8) and oriented with the dorsal region (expression area) on the right.
743 Dotted lines represent tissue outline defined by Actin staining (Figure S8). Blue arrows
744 indicate apical-lateral localization, orange arrows indicate medial-lateral localization. (A-
745 B) Localization of Nrx and Cora in *Ap* > *kune*^{RNAi} expressing discs at (A) 92h and (B) 116h
746 AED. In the portion of the disc without *kune*^{RNAi} expression Nrx is apical-laterally localized
747 at 92h and 116h AED, without medial-lateral localization. Nrx intensity localization is lost
748 with *kune*^{RNAi} expression at both times, but at 92h AED, also becomes more diffusely
749 localized. Cora localization is independent of Kune at 92h AED, but is lost with *kune*^{RNAi}
750 expression at 116h AED. (C-D) Localization of Kune and Cora in *Ap* > *nrx*^{RNAi} expressing
751 discs at (C) 92h and (D) 116h AED. Kune localization is lost with *nrx*^{RNAi} expression at
752 both times. Cora localization is independent of Kune at 92h AED, but is lost with *kune*^{RNAi}
753 expression at 116h AED. Cora localization is independent of Kune at 92h AED, but is
754 significantly diminished, although not completely lost, with *kune*^{RNAi} expression at 116h
755 AED. (E-F) Localization of Kune and Nrx in *Ap* > *cora*^{RNAi} expressing discs at (E) 92h and
756 (F) 116h AED. Kune and Nrx localization are lost with *cora*^{RNAi} at both times. (G) Summary
757 of imaging data, dotted line represents a cell membrane. (A-F) Images are representative
758 from n = (A) 8, (B) 10, (C) 8, (D) 6, (E) 5, and (F) 11 images.
759

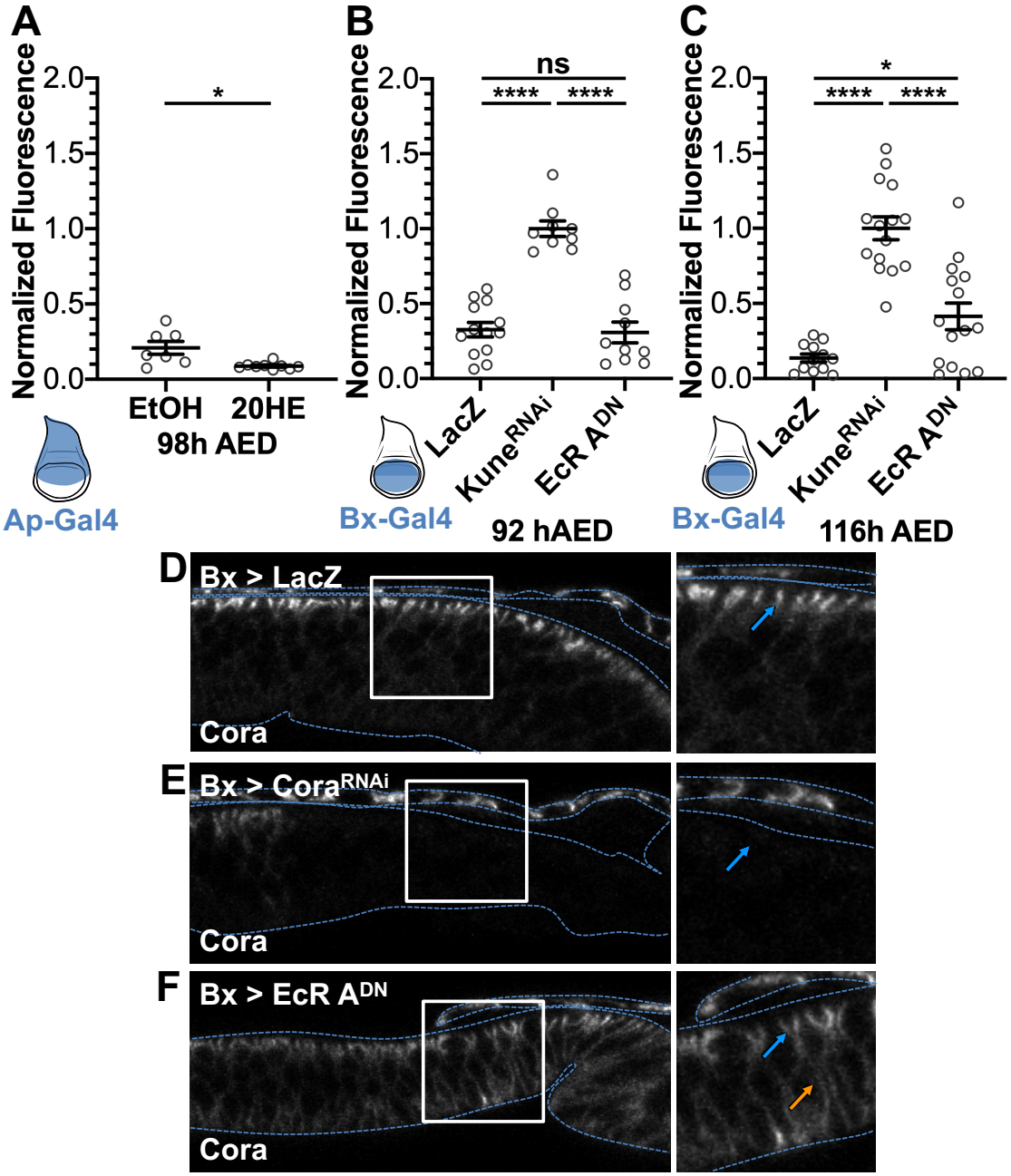

Figure 6. Ecdysone induces barrier maturation and Cora localization. (A) Function of the epithelial barrier at 98h AED in the wing imaginal discs of larvae that were switched to food containing ethanol control (EtOH) or 0.6 mg/mL 20-hydroxecdysone (20HE) at 80h AED. Barrier function is normalized to *Ap* > *kune*^{RNAi} expressing discs under the same feeding conditions (complete data in Figure S9B). Expression area diagramed in blue. (B-C) Epithelial barrier function of *Bx* > *lacZ* (wild type control), *Bx* > *kune*^{RNAi}, and *Bx* > *EcR A*^{DN} at (B) 92h and (C) 116h AED. Barrier function is normalized to *Bx* > *kune*^{RNAi}

768 expressing discs under the same feeding conditions. Expression area diagramed in blue.
769 (D-F) Localization of Cora in (D) *Bx* > *lacZ* (wild type control), (E) *Bx* > *kune*^{RNAi}, and (F)
770 *Bx* > *EcR A*^{DN} at 116h AED. Dotted lines indicate tissue outline as defined by actin staining
771 (rhodamine phalloidin; Figure S10). Tissues are oriented with the dorsal region of the
772 pouch (higher level of Bx expression) on the right. White box indicates zoomed area to
773 the right. Blue arrows indicate apical-lateral Cora localization (or lack thereof in *cora*^{RNAi}),
774 orange arrow indicates medial-lateral localization. (A-C) Graphs represent mean ± SEM,
775 with individual points indicating values of single images. Left to right, n = (A) 7 and 9, (B)
776 13, 8, 10, and (C) 12, 15, 15. (A-C) ns not significant, * $p < 0.05$, **** $p < 0.0001$ as
777 calculated by (A) Unpaired t-test with Welch's correction, (B) Ordinary one-way ANOVA
778 with Tukey's multiple comparisons test, or (C) Brown-Forsythe and Welch ANOVA tests
779 with Dunnett's T3 multiple comparisons test. (D-F) Images are representative of n = (D)
780 7, (E) 7, and (F) 5 images.
781

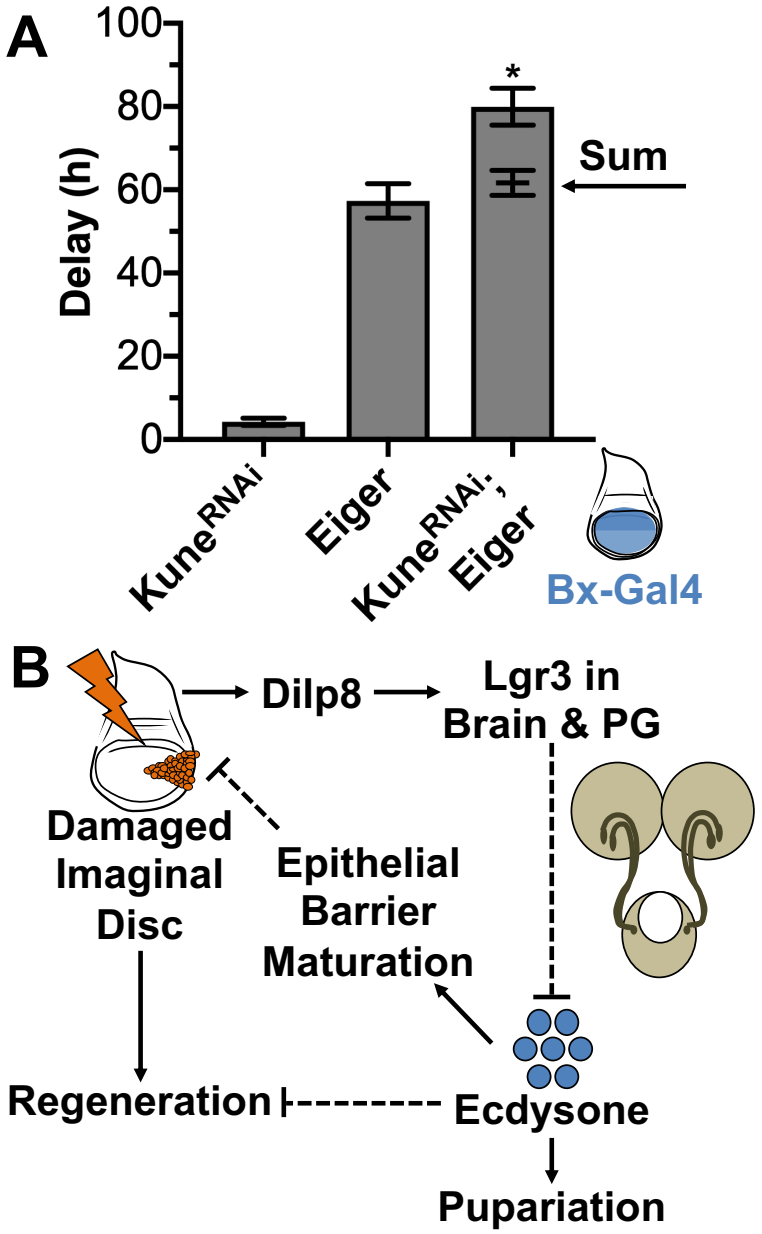

782

783 **Figure 7.** The epithelial barrier regulates the end point of regeneration. (A) Expression of
784 *kune*^{RNAi} in eiger-damaged tissues induces synergistic delay. Data were collected from at
785 least three independent experiments, bars represent mean ± SEM, * $p < 0.05$ from one
786 sample t-test comparing the additive value and observed delay. (B) Model. Following
787 damage to the imaginal discs, regeneration is initiated and Dilp8 is produced in the
788 damaged tissues and is secreted. Dilp8 functions on Lgr3 receptors in the brain and PG
789 to inhibit ecdysone production, resulting in a delay to pupariation. In the late third instar,
790 high levels of ecdysone inhibit regenerative ability and also induce the maturation of the

791 epithelial barrier in imaginal discs. The epithelial barrier inhibits Dilp8 signaling and
792 regulates the duration of the regeneration checkpoint in development. We hypothesize
793 that the restoration of the barrier following regeneration begins to limit Dilp8 release from
794 the wing disc, and that this is the rate-limiting step for ending the regeneration checkpoint.
795

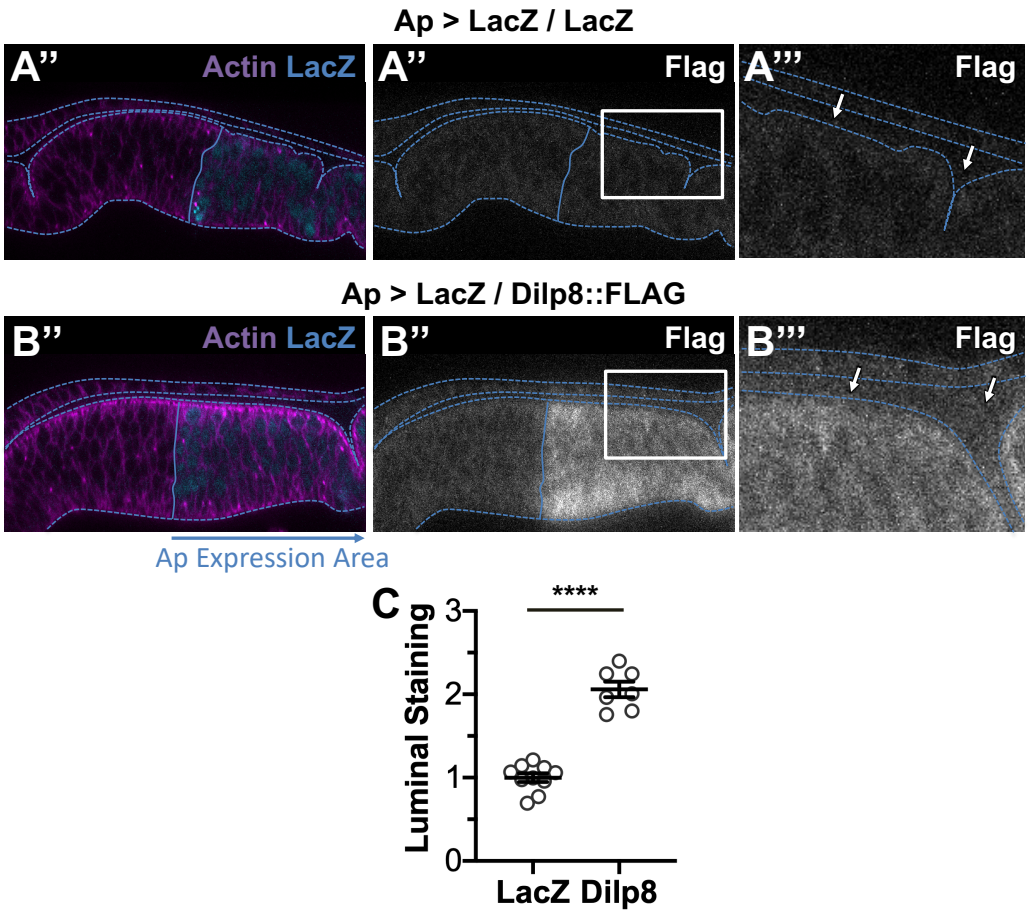

Figure S1. Dilp8 accumulates in the wing imaginal disc lumen. Ap-Gal4 was used to express (A) LacZ (wild type control) or (B) LacZ and Dilp8::FLAG in the dorsal region of wing imaginal discs. (A-B) Images are XZ cross-sections of wing imaginal discs in the pouch region of the disc. Dotted blue lines indicate disc area as defined by Actin (rhodamine phalloidin staining). Solid blue lines indicate the dorsal-ventral boundary, as defined by LacZ expression (β-Gal staining). Representative images are oriented dorsal on the right. (A) No FLAG is observed in *Ap > lacZ / lacZ* expressing discs either in (A'') the expression region or (A''') the lumen. (B) FLAG is observed in *Ap > lacZ / dilp8::FLAG* expressing discs in the (B'') expression region and (B''') the lumen. (C) Quantification of FLAG in the lumen, normalized to *Ap > LacZ* expression. Graph represent mean ± SEM, with individual points indicating values of single images. n = (LacZ) 10 and (Dilp8) 7 discs. **** $p < 0.0001$ by unpaired t-test.

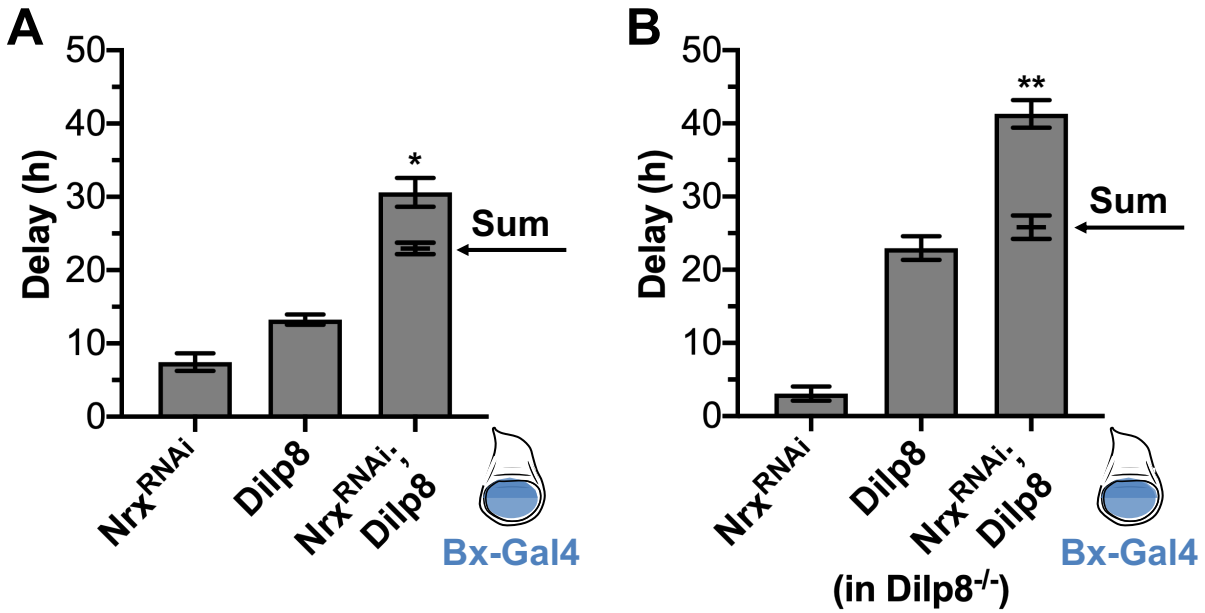

Figure S2. The epithelial barrier limits Dilp8 signaling. (A) Co-expression of *nrx*^{RNAi} and Dilp8 induces synergistic delay. Ectopic expression of nrx^{RNAi}, Dilp8, and co-expression of *nrx*^{RNAi} and Dilp8 (*nrx*^{RNAi}; Dilp8) induce developmental delay compared to LacZ controls when expressed in the wing imaginal disc under Bx-Gal4 (expression region in blue). The delay induced by co-expression of *nrx*^{RNAi} and Dilp8 (*nrx*^{RNAi}; Dilp8) is significantly more than the sum of the delay induced by *nrx*^{RNAi} and Dilp8 expressed alone (sum indicated by arrow). (B) This trend holds true when endogenous Dilp8 is limited by expression in a Dilp8 hypomorphic background (Dilp8^{MI00727}/Dilp8^{MI00727}; Garelli et al., 2012). Data were collected from at least four independent experiments, bars represent mean ± SEM, * $p < 0.05$, ** $p < 0.01$ from one sample t-test comparing the additive value and observed delay.

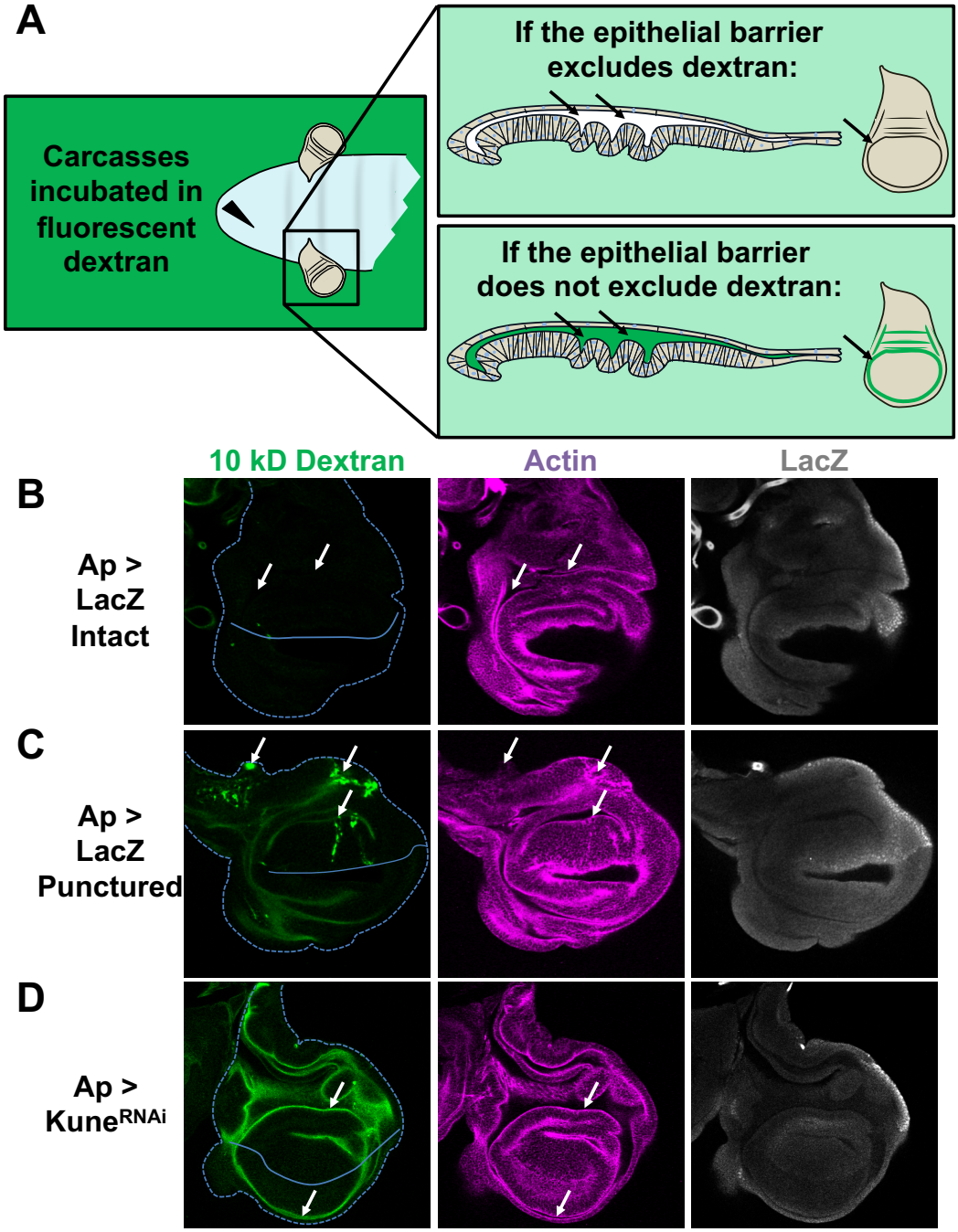

Figure S3. Explanation of the dextran assay for barrier function. (A) Carcasses are inverted and cleaned, then incubated in a fluorescence conjugated dextran for 30 minutes before fixation, the discs were then stained, mounted, and imaged (full description in methods). If the epithelial barrier excludes the dextran, no dextran should be observable in the lumen of the imaginal disc. If the epithelial barrier does not exclude the dextran or the tissue integrity is disrupted, dextran should be observable in the lumen. (B-D)

830 Representative images after 10 kD fluorescein-conjugated dextran incubation (from the
831 experiment quantified in Figure 2A). Ap-Gal4 was used to express LacZ (Ap > LacZ) or
832 $Kune^{RNAi}$ (Ap > $Kune^{RNAi}$). Dextran is observed in discs punctured LacZ expressing discs
833 (C) and $Kune^{RNAi}$ expressing discs (D), but not in intact LacZ expressing discs (A). Disc
834 area is indicated by the dashed line, as defined by Actin staining (rhodamine phalloidin).
835 Area of expression is dorsal (oriented up) of the solid line, as defined by LacZ staining (b-
836 Gal; note that LacZ expressing discs express two copies of LacZ while $Kune^{RNAi}$
837 expressing discs have one copy so β-Gal staining is not comparable between images).
838 Arrows indicate: (A) areas of the lumen with no distinguishable dextran fluorescence; (B)
839 areas where damage during dissection (puncturing) has disrupted epithelial barrier
840 integrity, allowing dextran to enter the cells and the imaginal disc lumen; and (C) luminal
841 dextran is observed in both the dorsal lumen ($Kune^{RNAi}$ expressing area, oriented up) and
842 also in the ventral lumen (non-expressing area, oriented down), indicating that the lumen
843 is contiguous. Images are single slices.
844

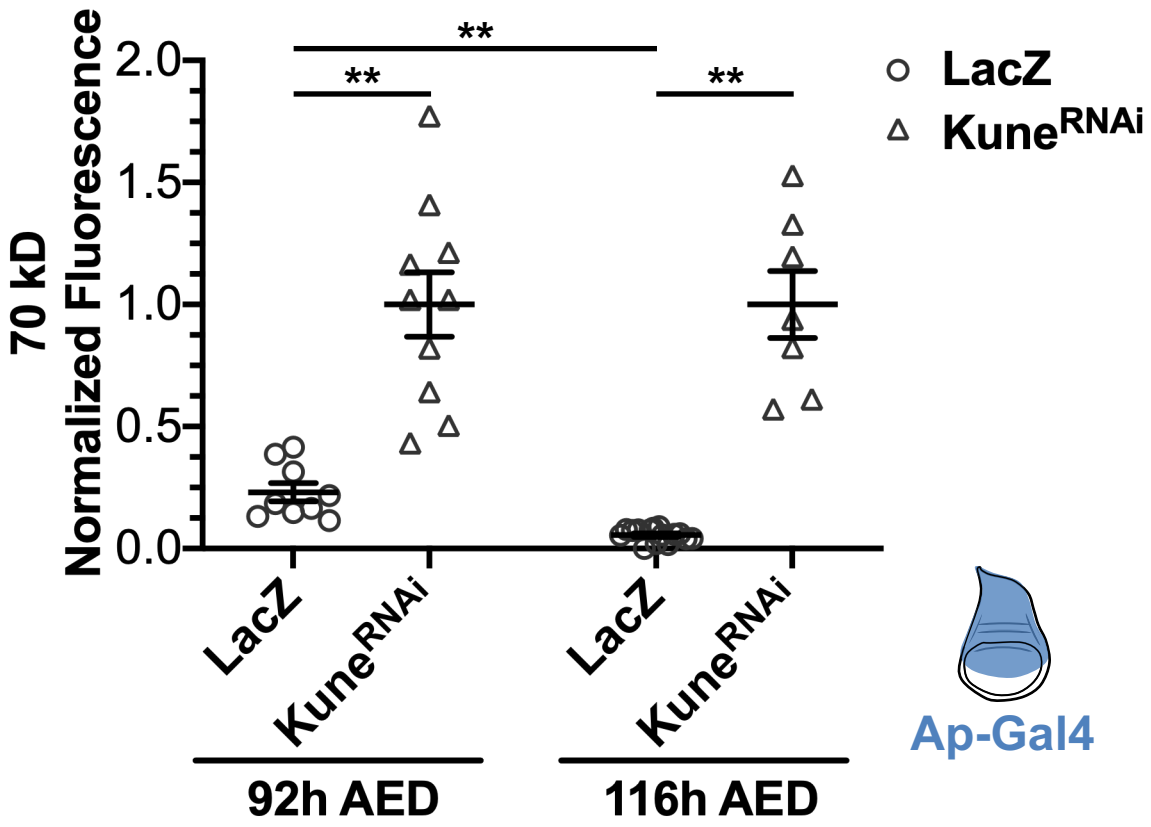

845

846 **Figure S4.** The epithelial barrier of wing imaginal discs grow more exclusionary to 70 kD
847 fluorescent dextran during the third instar. The function of the epithelial barrier to exclude
848 70 kD Texas Red conjugated dextran was measured, as previously described, at 92h and
849 116h AED in wing imaginal discs expressing LacZ or Kune^{RNAi} by Ap-Gal4 (expression
850 area diagramed in blue). Data are normalized to the mean luminal intensity of the
851 Kune^{RNAi} expressing discs. Graph represents mean ± SEM, with individual points
852 indicating values of single images. Left to right, n = 9, 10, 15, 7. ** $p < 0.01$ as calculated
853 by Brown-Forsythe and Welch ANOVA with Dunnett's T3 test for multiple comparisons.

854

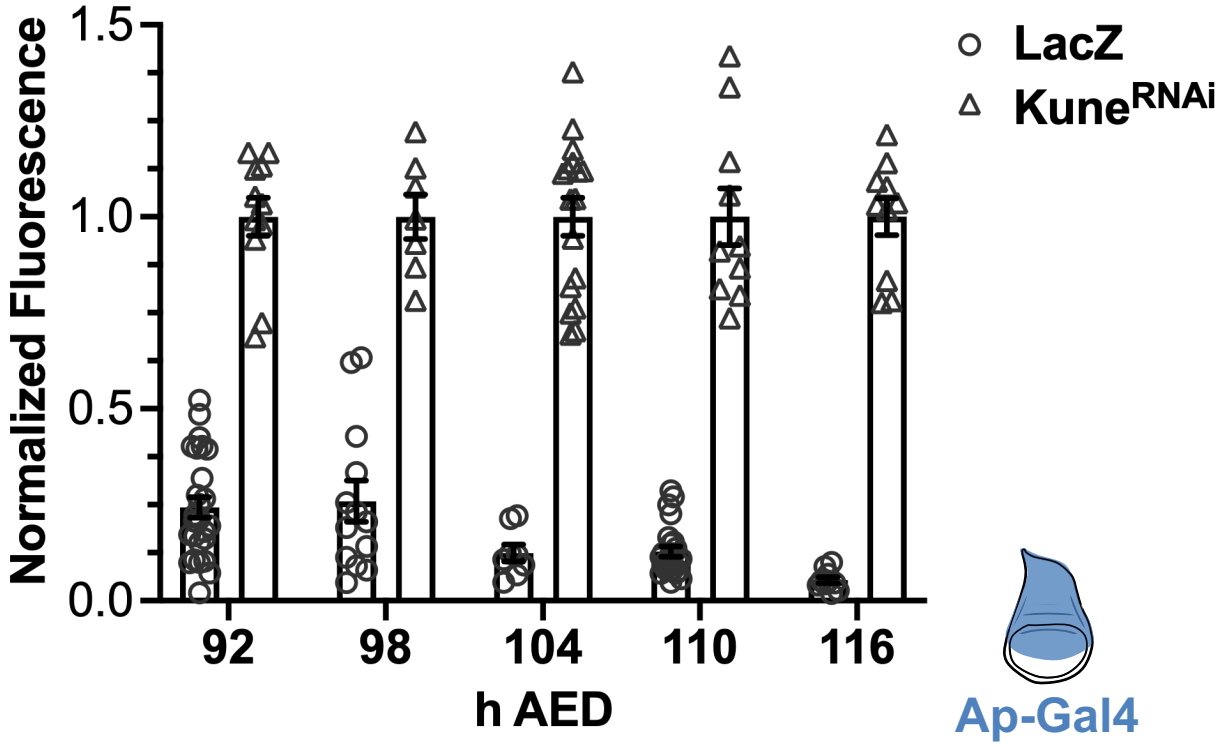

855

856 **Figure S5.** The epithelial barrier matures between 92h and 116h AED, becoming more
857 restrictive to 10 kD fluorescein conjugated dextran. These are the complete data from
858 Figure 2C, including data from Kune^{RNAi} expressing discs: the barrier function of wing
859 imaginal discs expressing LacZ or Kune^{RNAi} by Ap-Gal4 was measured every 6 hours
860 between 92h and 116h AED. Data indicate luminal intensity of intact LacZ expressing
861 discs normalized to the mean luminal intensity of the Kune^{RNAi} expressing discs from the
862 same timepoint. Graphs represent mean ± SEM, with individual points indicating values
863 of single images. Significance between LacZ expressing discs at each timepoint is
864 indicated in Figure 2C. Left to right, n = (92h AED) 26, 11, (98h AED) 13, 7, (104h AED)
865 12, 17, (110h AED) 25, 10, (116h AED) 10, 11.

866

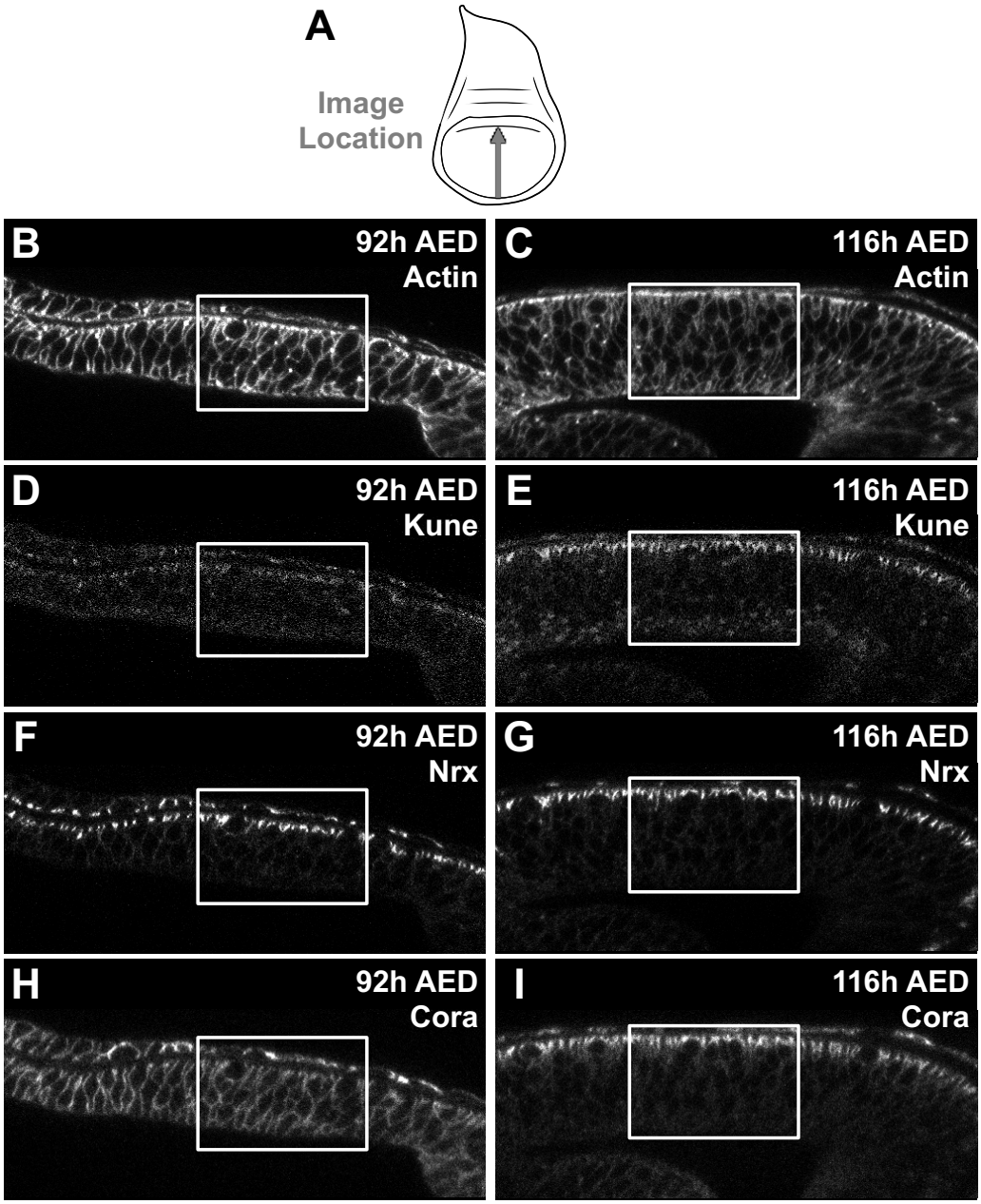

Figure S6. Complete images from Figure 3. (A) Approximate area and orientation of XZ image locations in the wing imaginal discs. (B-I) Representative XZ images at 92h and 116h AED, the region zoomed into in Figure 3 is indicated (white box). Images are: (B-C) Actin (rhodamine phalloidin; corresponds to Figure 3 B-C), (D-E) Kune (Anti-Kune; corresponds to Figure 3 E-F), (F-G) Nrx (Nrx-GFP; corresponds to Figure 3 G-H); and (H-I) Cora (Anti-Cora; corresponds to Figure 3 J-K).

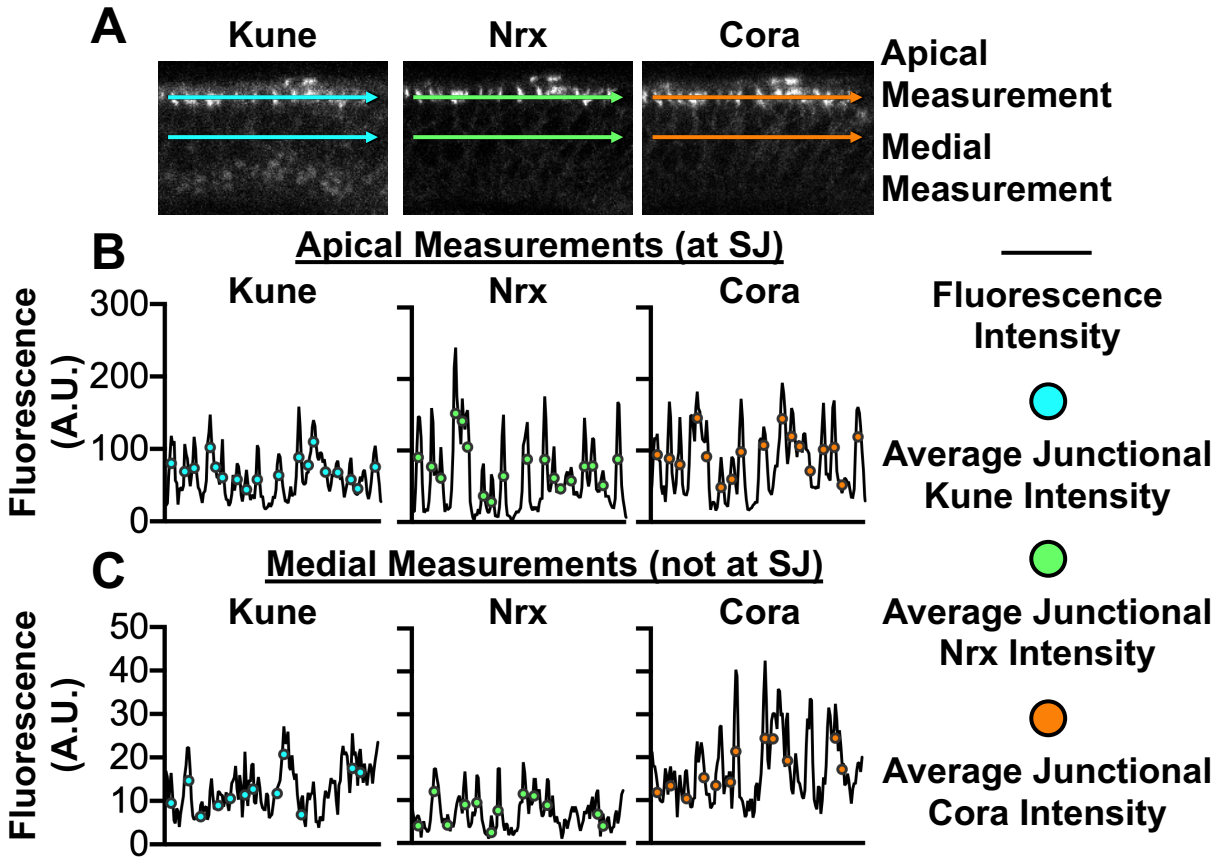

Figure S7. Method for junction quantification. (A) Lines were drawn apically bisecting the region of brightest septate junction (SJ) staining, and medially. (B-C) Fluorescence intensity across each line were measured with plot profile. Areas of the membrane (septate junction if apical) were identified as local maxima (peak) within a 7-pixel range, the 3 prior and following the pixel in questions. We adjusted these data in three steps, further described in Materials and Methods, to reduce false identification of a peak being localized at a membrane due to imaging or staining issues (eg. non-specific staining, image noise), especially with regards to Anti-Kune and Anti-Cora staining. The average junctional intensity was taken as the mean of the 7-pixel range.

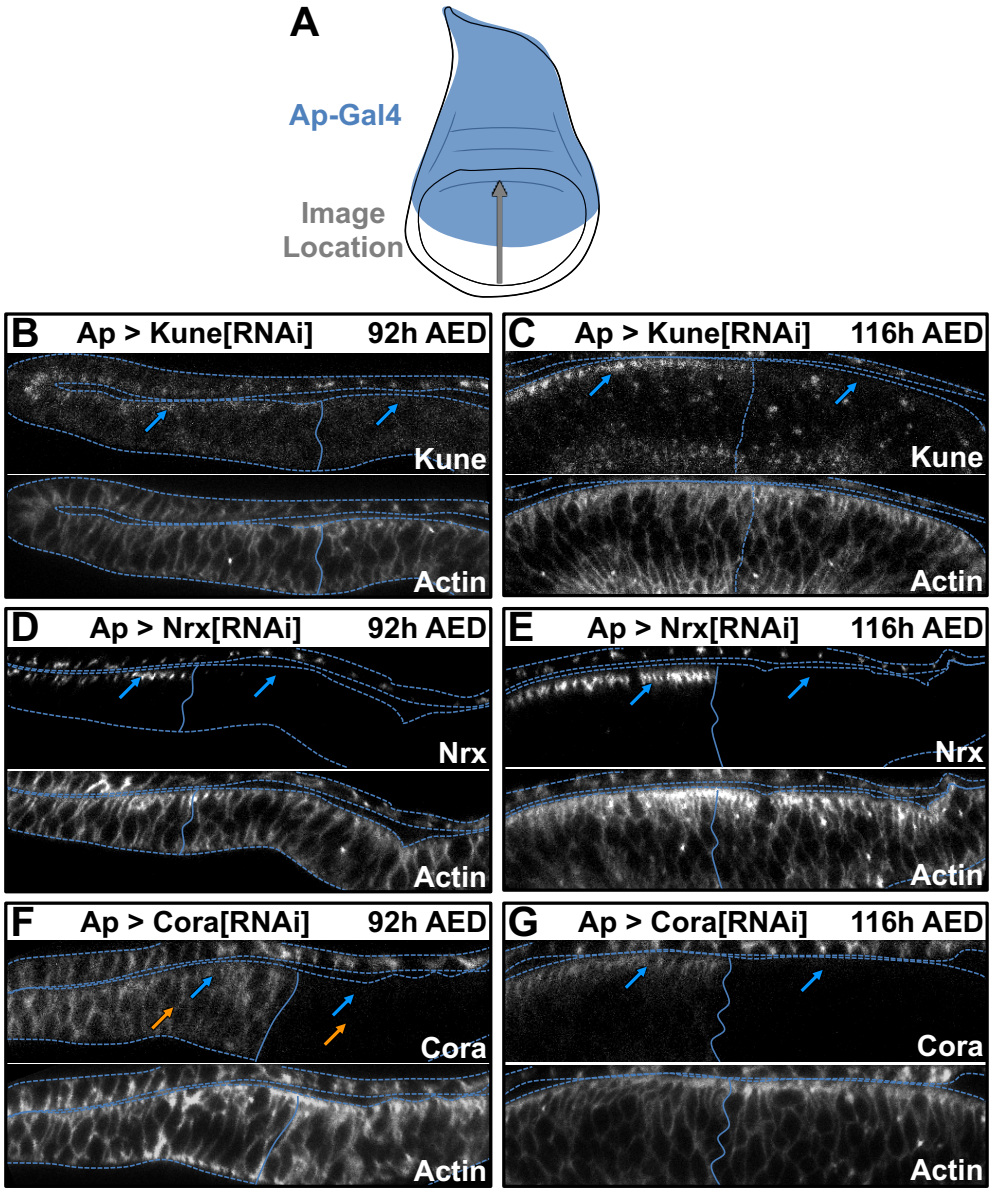

Figure S8. RNAi inhibition of septate junction components. (A) Images were taken spanning the dorsal-ventral boundary in the pouch region of wing imaginal discs (approximate area indicated by grey arrow), which includes tissue outside and inside the Ap-Gal4 expression region (blue). (B-G) Localization of septate junction components following RNAi expression and actin localization (defined by rhodamine phalloidin). Images are from the same discs as Figure 5. Dotted line represents tissue outline defined by actin staining. Solid line represents dorsal-ventral boundary, expression area (dorsal region) is on the right. Blue arrows indicate apical-lateral localization, orange arrows indicate medial-lateral localization. (B-C) Localization of Kune and Actin in *Ap* > *kune*^{RNAi}

897 expressing discs at (B) 92h and (C) 116h AED. Kune is depleted in the *kune*^{RNAi}
898 expression region at both times. Images are of the same discs as Figure 4A and 4B. (D-
899 E) Localization of Nrx and Actin in *Ap* > *nrx*^{RNAi} expressing discs at (D) 92h and (E) 116h
900 AED. Nrx is depleted in the *nrx*^{RNAi} expression region at both times. Images are of the
901 same discs as Figure 4C and 4D. (F-G) Localization of Cora and Actin in *Ap* > *cora*^{RNAi}
902 expressing discs at (F) 92h and (G) 116h AED. Kune is depleted in the *cora*^{RNAi}
903 expression region at both times. Images are of the same discs as Figure 4E and 4F.
904

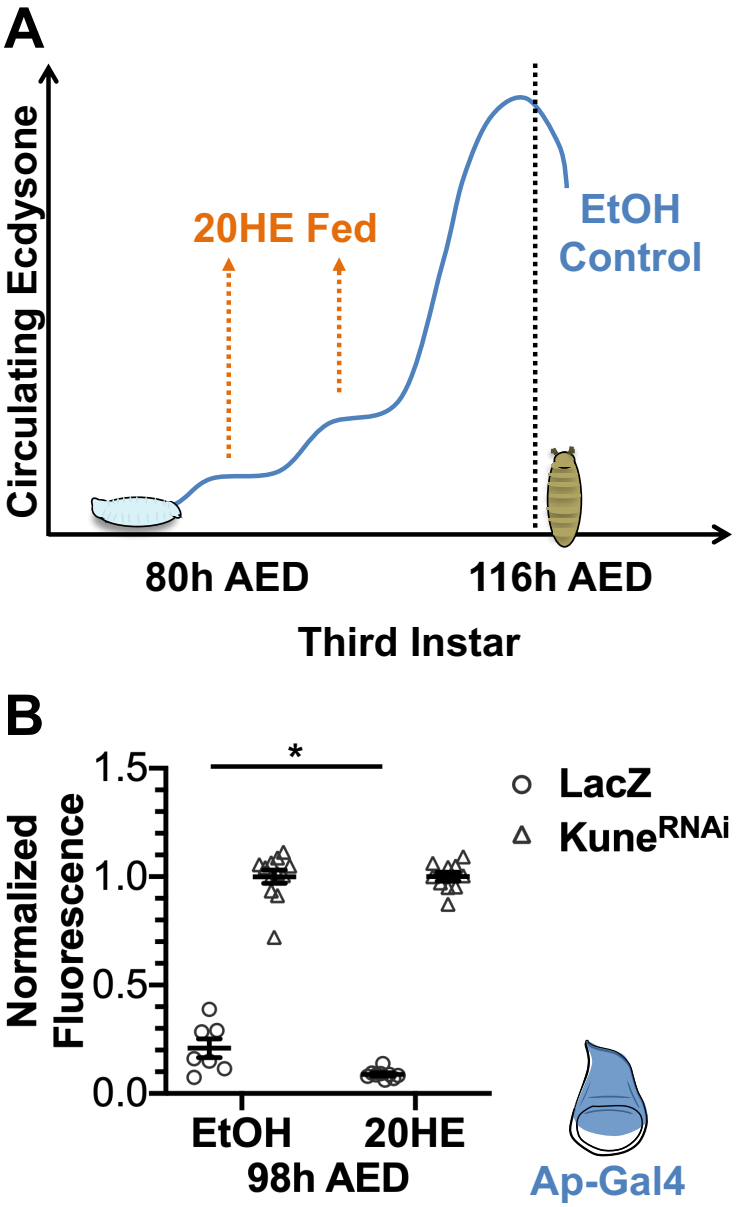

905

906 **Figure S9.** Ecdysone feeding induces barrier maturation early. (A) At 80h AED, larvae
907 were switched to food containing 0.6 mg/mL 20-hydroxyecdysone (20HE) or ethanol
908 control (EtOH). Feeding 0.6 mg/mL 20HE at 80h AED does not influence pupariation time,
909 but does limit regeneration (Colombani et al., 2005; Jaszczak et al., 2015). (B) Wing
910 imaginal disc barrier function at 98h AED of larvae fed the EtOH or 20HE food. Data are
911 from larvae expressing *Ap* > *lacZ* (data in Figure 6A) or *Ap* > *kune*^{RNAi}. Expression area
912 indicated in blue. Graph represents mean ± SEM, with individual points indicating values

913 of single images. Left to right, n = 7, 12, 9, 10. * $p < 0.05$ as calculated by unpaired t-test
914 with Welch's correction.
915

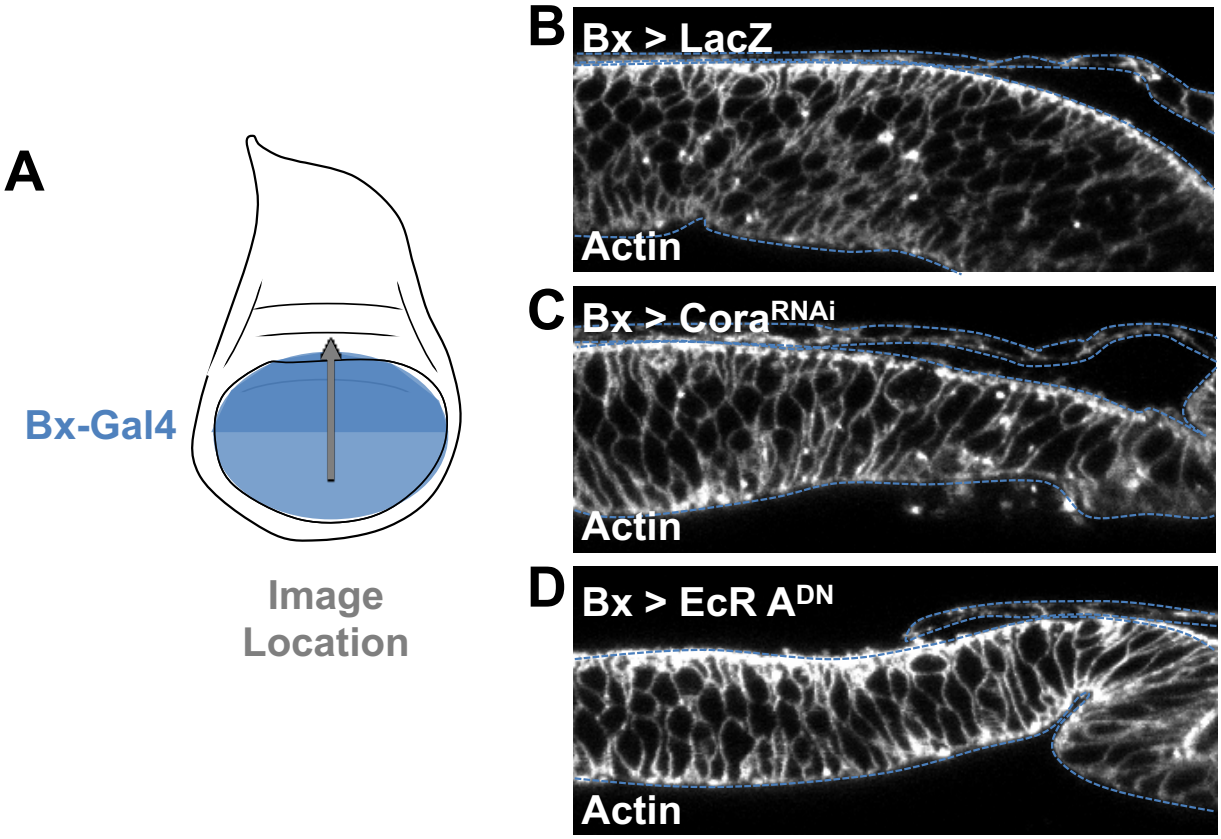

Figure S10. Actin stain from discs in Figure 6. (A) Bx-Gal4 expression area (blue) and approximate image location (grey arrow) for B-D. (B-D) Localization of Actin (rhodamine phalloidin) in (B) *Bx > lacZ* (wild type control), (C) *Bx > kune*^{RNAi}, and (D) *Bx > EcR A*^{DN} at 116h AED. Dotted lines indicate tissue outline. Tissues are oriented with dorsal on the right. Images are from the same discs as Figure 6D-F.

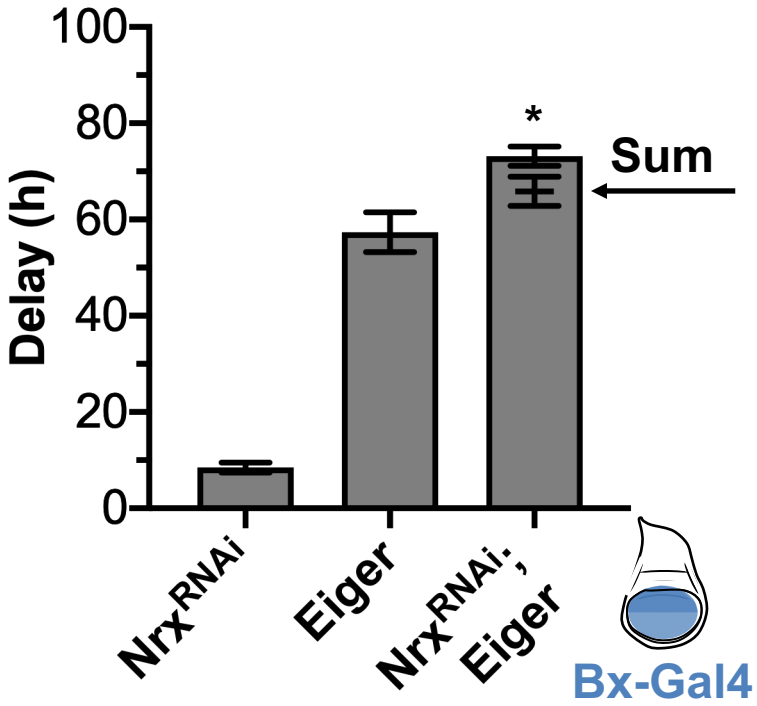

923

924 **Figure S11.** Nrx limits Eiger-induced delay. Co-expression of *nrx*^{RNAi} and Eiger produces
925 synergistic delay. Ectopic expression of *nrx*^{RNAi}, Eiger, and co-expression of *nrx*^{RNAi} and
926 Eiger (*nrx*^{RNAi}; Eiger) induce developmental delay compared to LacZ controls when
927 expressed in the wing imaginal disc under Bx-Gal4 (expression region in blue). The delay
928 induced by co-expression of *nrx*^{RNAi} and Eiger (*nrx*^{RNAi}; Eiger) is significantly more than
929 the sum of the delay induced by *nrx*^{RNAi} and Eiger expressed alone (sum indicated by
930 arrow. Data were collected from at least four independent experiments, bars represent
931 mean ± SEM, * $p < 0.01$ from one sample t-test comparing the additive value and
932 observed delay.

933

934

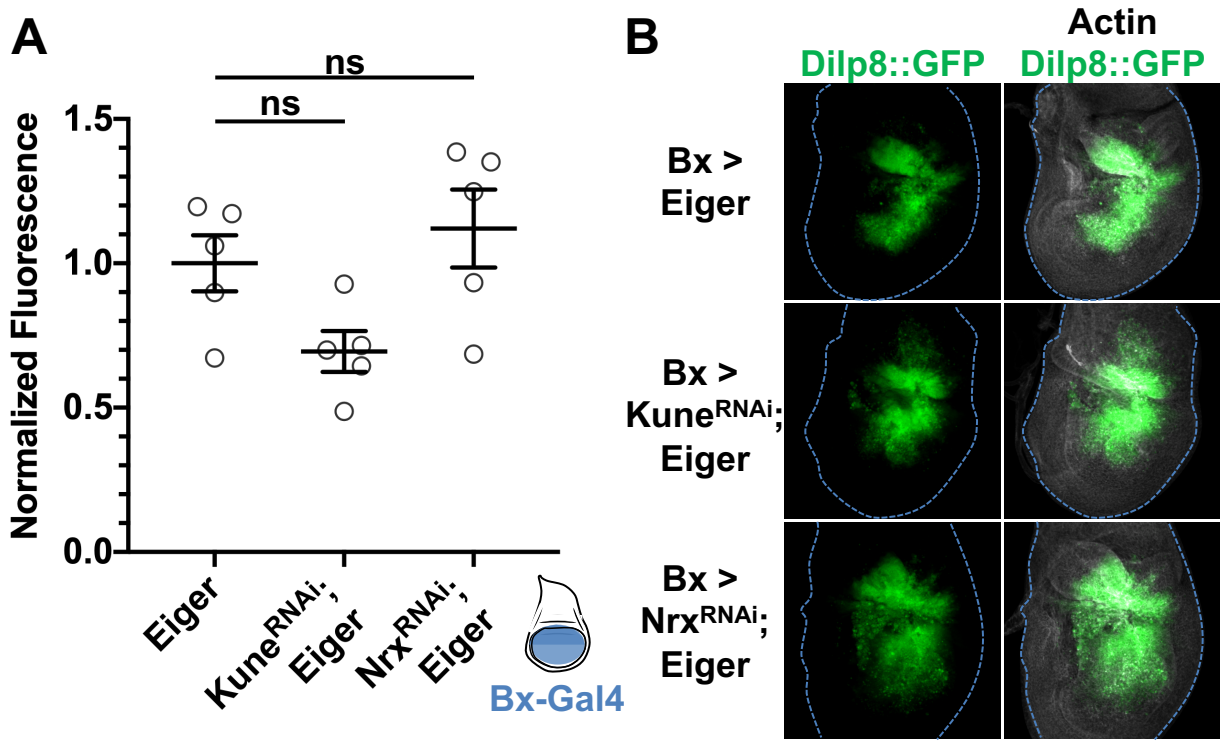

935

936 **Figure S12.** Coexpression of Eiger and RNAi against septate junction components does
937 not significantly alter measured Dilp8 expression. Bx-Gal4 (expression area in blue) was
938 used to express Eiger alone, with *kune*^{RNAi}, or with *nrx*^{RNAi} expressing a transcriptional
939 reporter for Dilp8 (Dilp8^{MI00727}/+; Garelli et al., 2012). (A) Sum GFP intensity was
940 measured and the data were normalized to Eiger alone. (B) Representative images. Discs
941 were collected at 104 hAED. Images represent sum-projected stacks of 5 images. Actin
942 was stained for with rhodamine phalloidin. (A) Graph represents mean ± SEM, with
943 individual points indicating values of single images, n = 5 images in each condition; ns
944 indicates $p > 0.05$ by one-way ANOVA with Tukey test for multiple comparisons.

945

946